Histologic Images Analysis

Samuele Dietler

School of Computer and Communication Sciences

Diploma project

Spring 2010

Supervisor
Prof. Jean-Philippe Thiran
EPFL / LTS5

Expert
Dr. Blaise-Julien Meyrat
CHUV

Contents

Chapter 1

Introduction

In the last decades, signal processing and more specifically image processing became more and more popular in several domains such as telecommunication and medical field. In the medical field, signal and image processing has known a huge expansion due to its broad range of applications and to the great help that these techniques bring to the medical staff. Image processing techniques are used to analyze all the types of medical images, from X-Ray to microscope images. Analysis can be "automatic", "semiautomatic" or "manual". The term "Automatic" indicates that all the processes are done by the routine/application/machine without any intervention of the user, "semiautomatic" means that some manipulation by the user are required and "manual" indicates that all the processes are done by the user.

In this project, image processing techniques are applied to images acquired by microscope in order to compute the density of the Cajal cells in the bowel. The images acquired by the microscope come from specimens of normal bowel harvested during oesocoloplasties. This small tissue is marked with a C-Kit antibody before it is visualized. The C-Kit marker gives a brown color to the Cajal cells. In order to compute the ratios of these cells, processing such contrast enhancement, smoothing, segmentation based on color and morphological operators should be applied. These densities are then used by the medical staff to try to find a relationship between the number of the Cajal cells in the ganglionic and aganglionic regions.

The first section of the report is dedicated to the general knowledge of the concept treated in this report such as a brief introduction of the Hirschsprung's disease (HD), Cajal cells and general terms concerning the image processing. The next two sections explain the segmentation and the stitching processes and discuss the obtained results. Then, the possible densities computation are discussed in chapter 4 followed by a section where the developed graphical user interface is presented. Finally, conclusions of the project and future work are presented.

1.1 Goal

The goal of this project is to develop an image processing tool helping to analyse the evaluation of the density of Cajal cells in presence or not of the HD. This tool works in a "semiautomatic"

way, requiring the user to modify a certain number of parameters in order to correctly estimate the values of the Cajal cells. The estimation of the density can be done in a single or multiple image. The computed density is then used by scientists to try to find a relationship between the aganglionic region causing the HD and the density of Cajal cells.

1.2 Hirschsprung's disease

Hirschsprung's disease (HD) [1], also called congenital aganglionic megacolon [14], is a congenital disease that causes intestinal obstruction. The disease is named Hirschprung because the first scientist to discover the symptoms was the physican Harald Hirschsprung in 1886. Intestinal obstruction results from an aganglionic region in the bowel of the newborn and can vary in length, going from the distal rectum to the proximal intestine [15]. This disease has an incidence of about 1:5000 newborn. In addition, the HD can be hereditary.

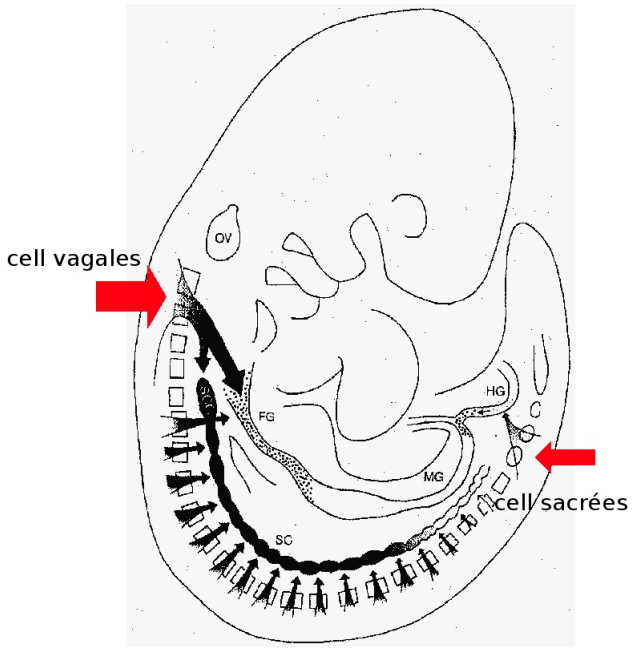

Figure 1.1: Vagal and sacral cells in a fetus [9]

The ganglionic cells are originated in the neural crest and migrate through the bowel, forming the enteric nervous system [8]. The enteric nervous system is responsible for the bowel motility and secretory activities. The ganglionic cells come from the vagal and from sacral cells (figure 1.1), but the vagal cells are considered more important (most of the cells come from vagal [1] cells). In a healthy fetus, starting from the 4th week of its growth, the vagal cells migrate along the bowel by genes factor and environment. This process produces two types of plexus : the myenteric plexus (which controls the motor activity [1] figure 1.2(a)) between the two internal and external muscular layers and the submucous plexus between the internal muscle layer and the mucosa (it controls the secretomotor function, figure 1.2(b)). During the migration phase, the cells multiply and differentiate (around 2000 neural crest cells form 500000 cells [9]).

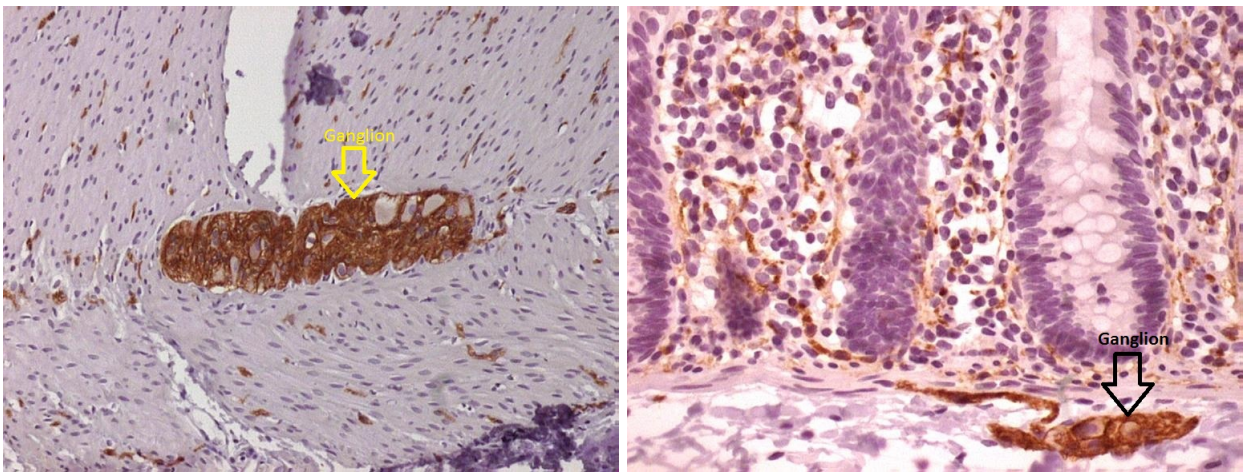

(a) Myenteric plexus (b) Submucous plexus

Figure 1.2: Two different types of plexus [8]

In the case of a newborn with Hirschsprung disease, the aganglionic region is due to the arrest of the migration of the neural crest cells. The aganglionic region is in the two plexus (figure 1.3 shows this situation). Above the aganglionic region there is a transition region where the ganglions become more and more rare. The transition to the aganglionic region produces the obstruction of the bowel and by consequence the region before the transition becomes larger than normal (figure 1.4). The earlier the migration stops, the longer the aganglionic region is and more severe is the disease. At the moment, there is no explanation on the cause of the disease and this subject is an active field of research.

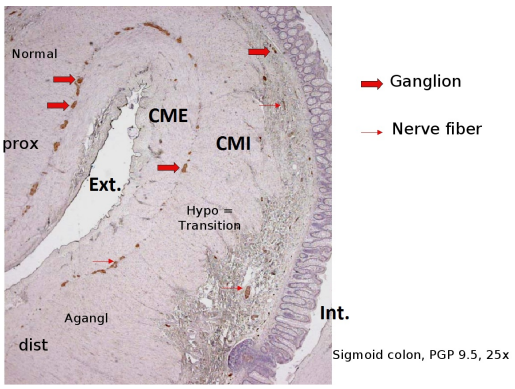

Figure 1.3: Transition zone [8]

The first symptoms indicating the presence of the disease can be the non-expulsion of the meconium within the 48 hours after the birth, constipation, abdominal distension,vomiting and enterocolitis. Enterocolitis is the most common cause of death in the HD. The diagnosis can be made by radiological studies with contrast product, recto-anal reflex and by histological examination of

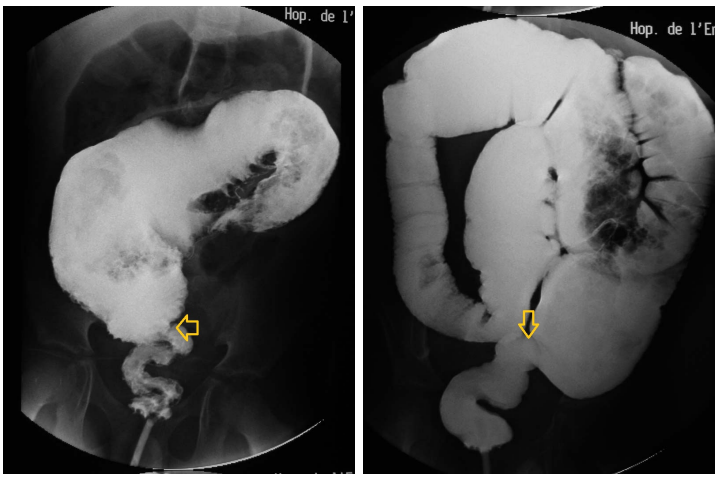

(a) (b)

Figure 1.4: Baryum enema [8] : arrow indicates the transition zone

the rectal wall by biopsy. The latter is the only way to be sure of the presence of the Hirschsprung disease and therefore this is the method used to acquire the Interstitial cells of Cajal.

1.2.1 Interstitial cells of Cajal

The Interstitial Cajal cells (ICC) are originated from the mesoderme and therefore are not nervous cells. These cells are developed at the same time as the enteric nervous system. The Cajal cells are located between the two muscular layers (myenteric plexus) and in the submucous plexus. At this time, Cajal cells are known to perfom three main activities :

- These cells act as pacemaker, generating electric waves that are used to move the bolus along bowel(figure 1.5). This action is called "Perstaltism" and is not possible if the Cajal cells are not present or if the cells are not bound with some others special cells;
- Facilitates the propagation of electrical events [4];
- Mediating neurotransmitter [4];

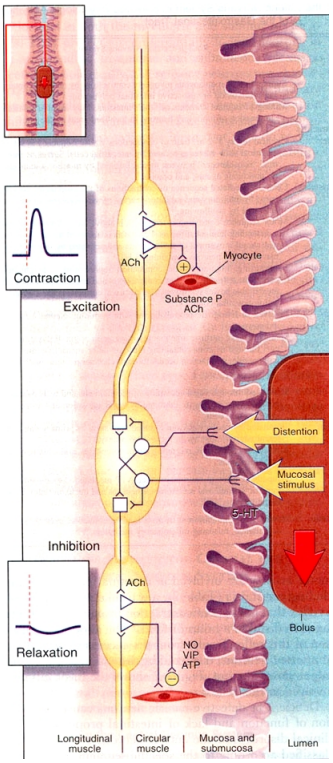

Figure 1.5: Motility [9]

The absence of ICC can provoke irregular electric waves (pacemaker property) on the bowel wall, causing a slow and uncontrolled motility. This can be the cause of the problems encountered in the Hirschsprung disease. At the moment, the relationship between these two actors is not clear : some studies have established a relation between the Cajal cells and the Hirschsprung whereas other do not find any relationship; this argument is still under debate and it is an active field of research.

The Interstitial cells can be recognized either by electron microscopy or by histological techniques applied with a classical microscope. The histological technique is used to capture images of the Cajal cells. The histological technique requires a biopsy of the bowel with the two plexus (muscle coats and submucosa) that should be present in the specimen. The C-Kit antibody is applied to the extracted small tissue of the bowel, this marker enhances the presence of the Cajal cells (figure 1.6 shows a C-Kit marked specimen) and therefore the number of these cells can be evaluated.

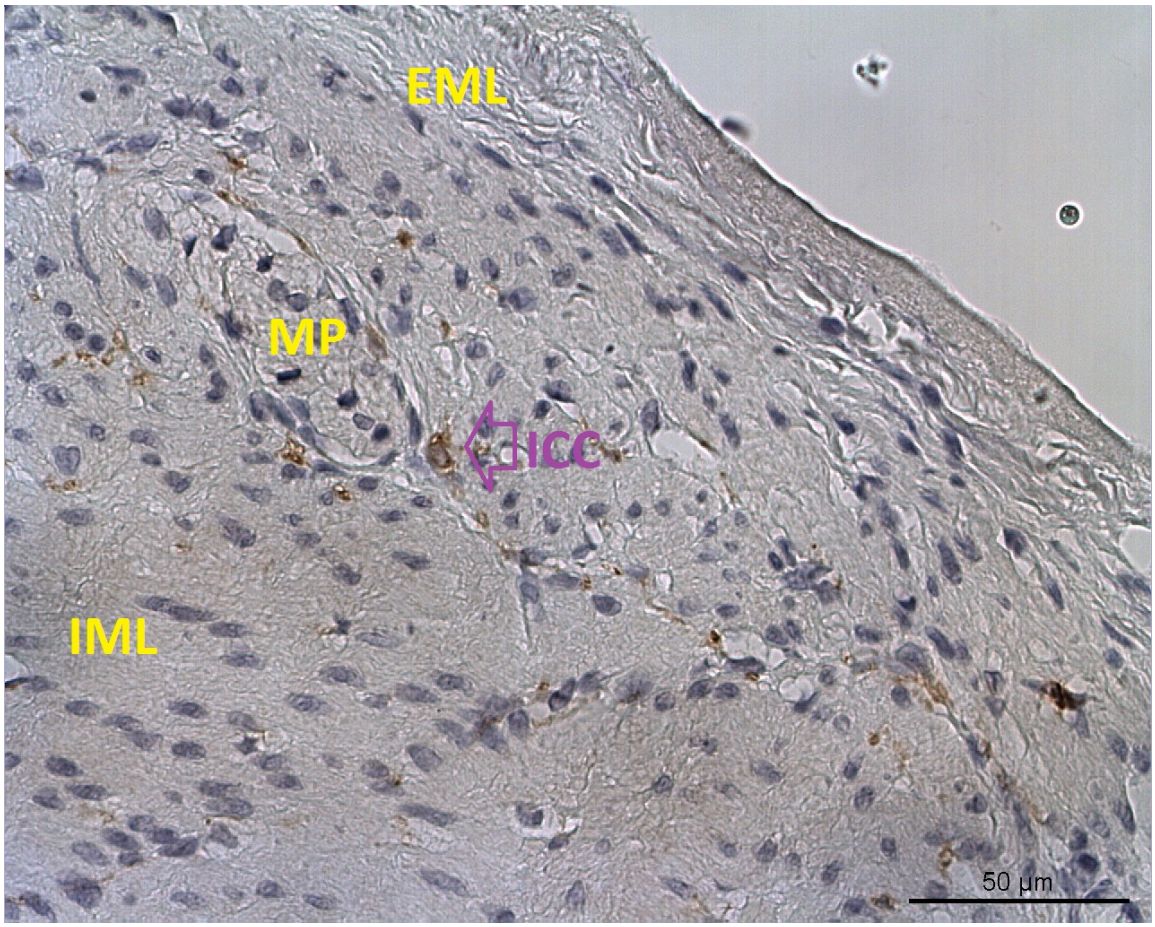

Figure 1.6: A colored C-Kit specimen captured with microscope. MP myenteric plexus, IML/EML internal/external muscle layer and ICC interstitial cell of Cajal

1.3 Image description

1.3.1 General definition of a grayscale image

A grayscale continous image can be defined as a two-dimensional function f(x,y), where (x,y) refers to the spatial coordinates of the image [10, 2]. The amplitude or the gray level of each pair of coordinates (x,y) is the brightness of the image at this point, and the range of intensities that this coordinates can have are defined as $f \in [f_{min}; f_{max}]$. The lower values represent dark luminosity

whereas the high values represent bright luminosity.

Today, most of the images are digital representations of continuous images, meaning that real world is sampled and quantized. Figure 1.7 shows a digital representation of a continuous image. Image sensors sense the real world and convert the luminosity of the scene into electrical signals, and these signals are transformed into numerical values becoming a digital image [2]. The values of such an image are finite discrete quantities and thus it can be considered as a finite array of pixels. Mathematically, the values of a discrete image are considered as part of $l_2\left(\mathbb{Z}^2\right)$ space where the $l2$-inner product is defined (Hilbert space).

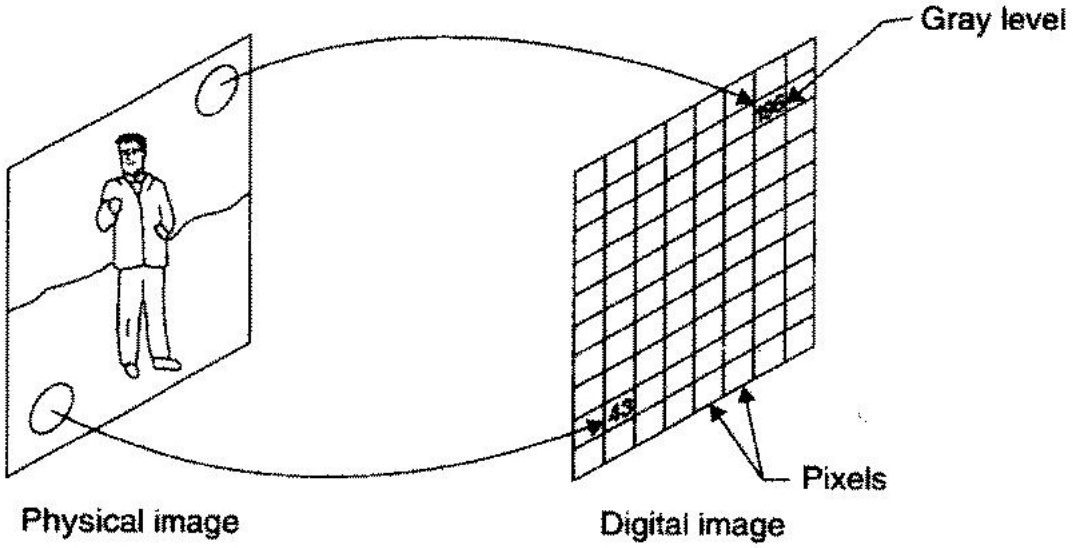

Figure 1.7: Digital image [10]

1.3.2 General definition of a RGB image

A RGB image is considered as a stack of three grayscale images representing the red, green and blue channels of an image. The pixels of such an image can be considered as 3D vectors in the RGB space. In figure 1.8 the RGB vector space is pictured. These three color channels are used because the human eye absorbs the light as a function of the wavelength by three different cones situated on the wavelength of the red, green and blue light. This topic is not treated in this report and interested readers can consult the book : "Digital Image Processing" [2] for more information.

1.3.3 Images acquired with microscope

The captured images are 8 bits color images, this means that each channel (red, green and blue) is encoded with 8 bits and therefore the intensity of a pixel in a single channel can range from 0 to 255.

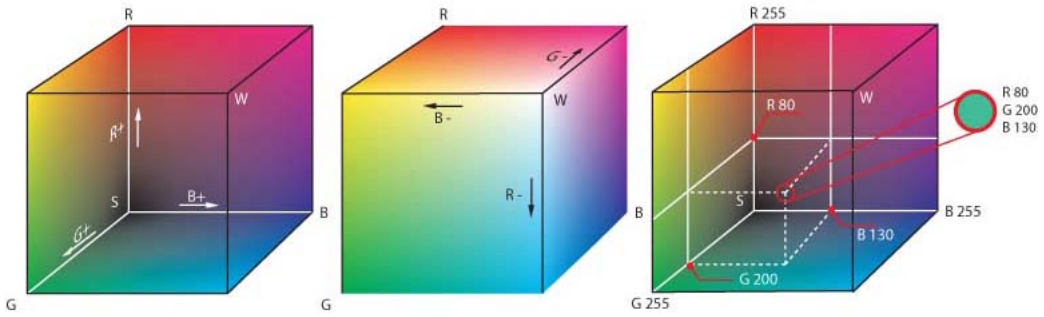

Figure 1.8: RGB space [21]

The microscope used for this project is a ZEISS "Axioscope". The camera used for acquisition on the microscope is a LEICA "DFC 280" with software LEICA "Image Manager 50" version 5 release 247.

1.4 Overview

Firstly, the image of a specimen is captured with a classical microscope. The specimen is divided in regions of interest and each region is captured with a magnification of 40 times in order to reveal as many details as possible. All the steps used to reveal and compute the density of the Cajal cells are reported in the figure 1.9. The acquired images are preprocessed to reduce the noise and to increase the performance of the segmentation. Subchapter 2.2 illustrates this process.

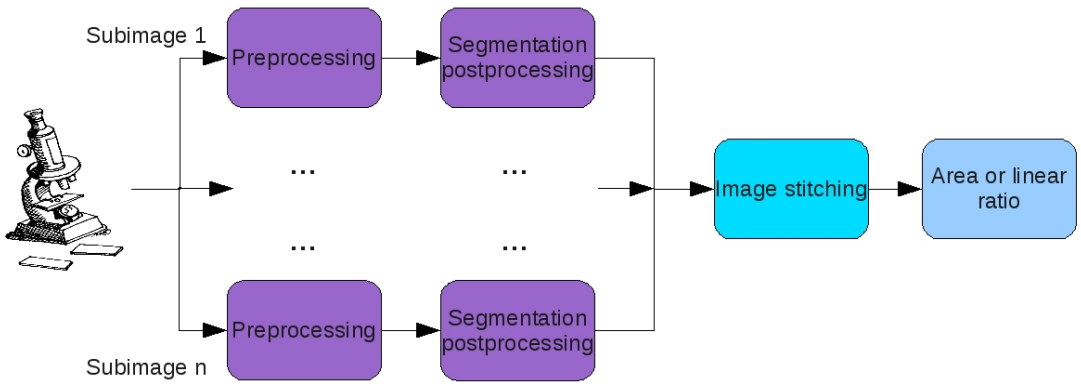

Figure 1.9: Processing steps to compute Cajal density

Secondly, the RGB segmentation is computed. This step discriminates the Cajal cells from all the other cells present in the image. The Cajal cells are postprocessed and a contour is drawn around each cell. Subchapters 2.3 to 2.4 present more detailed information about these steps.

The next step consists on binding all the images together in order to reconstruct the interesting region to analyze. This step is not mandatory and can be avoided if the user is interested only in a single region of the global image. Image stitching applied to the Cajal cells is presented in subsection 3.3.

Finally, the density of the Cajal cells is computed. There are two possible ratios, the first ratio is between the area of the Cajal cells and the total area of the image, the second density is a ratio between the area of the Cajal cells and the length of a line that passes in between the two plexus. These two density computations are illustrated in chapter 4. All the processing and development are made in Matlab and a standalone application is created for redistribution.

Chapter 2

Preprocessing, segmentation and postprocessing techniques

2.1 Introduction

This chapter is dedicated to the preprocessing, segmentation and postprocessing techniques applied to reveal the Cajal cells. Therefore, a detailed explanation of the image processing flow (violet part on figure 1.9) is discussed. The image processing workflow for Cajal cell discrimination is reported in figure 2.1.

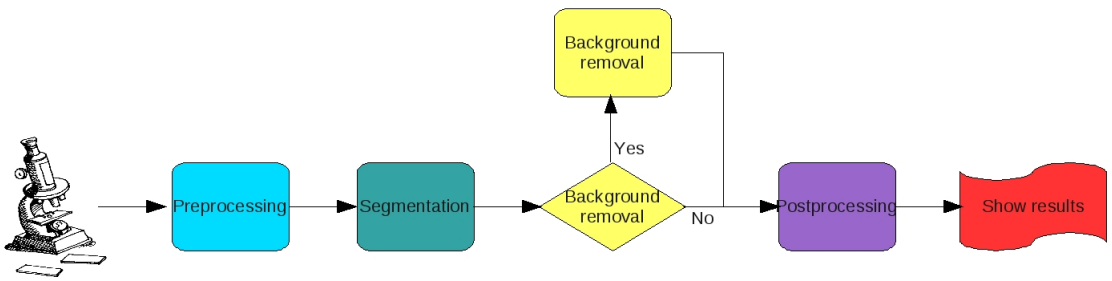

Figure 2.1: Processing workflow

The images captured by the microscope are firstly preprocessed by an enhancement algorithm to increase the contrast between the Cajal cells and the surrounding background. In the same stage of the contrast enhancement, a smoothing filter that preserves the edges is applied to increase the uniformity across the regions. Next, a segmentation algorithm based on color discrimination is used to reveal Cajal cells. Finally, morphological operators are applied to enhance the quality of the segmentation and to remove noisy areas in the image.

The structure of this chapter follows the processing pipeline, the first subchapter describes the techniques used for the preprocessing tasks. After, a discussion on segmentation is presented followed by the morphological operators. Finally, area validation based on comparison between the "manual" segmentation done by expert user and segmentation computed by our application is done.

2.2 Preprocessing techniques

Preprocessing is usually a relevant step and can highly increase the results of segmentation. In our processing flow, preprocessing is used as a contrast enhancement and smoothing step. Figure 2.2 shows the preprocessing steps, whereas figure 2.4 shows the resulting images after each block of the workflow.

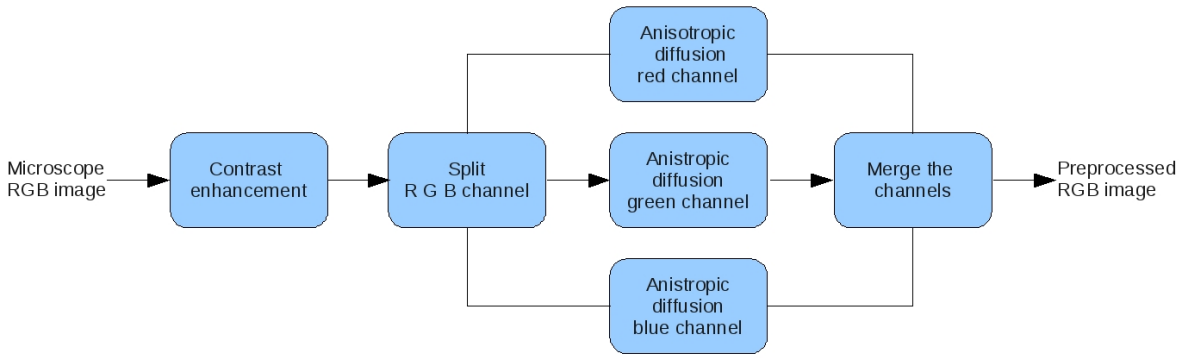

Figure 2.2: Preprocessing workflow

Contrast enhancement (figure 2.4(b)) is computed by mapping the intensity values of the microscope image (figure 2.4(a)) to a new intensity image such that a certain amount of intensity values are saturated at low and high intensity. 10 % of the intensities are saturated at low and high value. Saturation means that values below and above the low and high threshold values are set to the lowest and highest possible value in the new image. The other intensities are linearly mapped on the new image, as reported in the formula 2.1 [16]. Figure 2.3 shows a possible linear mapping.

$$I_{new}(x,y) = I_{newlow} + (I_{newhigh} - I_{newlow}) * \frac{I_{old}(x,y) - I_{oldlow}}{I_{oldhigh} - I_{oldlow}} \tag{2.1}$$

Smoothing is done by an anisotropic diffusion filter (figure 2.4(c)), this filter permits to smooth the image while preserving the edges. The mathematical details of this filter are not discussed in this report, therefore interested readers can find relevant information on the paper "Scale-space and edge detection using anisotropic diffusion" [5]. Although, other smoothing filters with faster

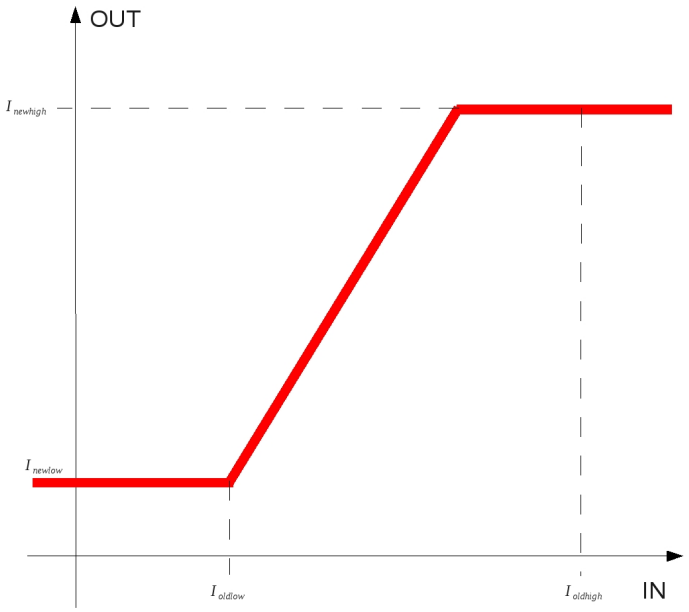

Figure 2.3: Linear intensity transformation

computation can be chosen, the anisotropic diffusion filter presents the advantage of preserving the edges and therefore the border of the cells remain well defined and do not become smoothed.

2.3 Image segmentation

Segmentation is the main core of this project and is done by color discrimination of the objects present in the image. The color based segmentation is computed by transforming the RGB color space into a grayscale image, with high intensity graylevel for the Cajal cells. As briefly discussed in chapter 1.3.2, the images can be considered as a vector space, therefore pixels in a RGB color image can be defined as 3D vectors in this space. Moreover, the segmentation is computed by projection of each RGB pixel into a new basis, resulting in a grayscale image. Color based segmentation is chosen instead of others segmentation techniques because Cajal cells have different color from the other objects in the image and do not have any particular shape that can be used as a feature.

2.3.1 Segmentation method

The coloration of the specimen is done by the C-Kit marker (more information can be found on the wiki webpage [11]), this marker allocates different colors to the different cells allowing a color discrimination among them. Each class of colors on the image have their own cloud of points in the RGB space, as figure 2.5 shows (this figure displays an ideal representation of two classes of colors in an image). The classes are discriminated by construction of a hyperplane that is perpendicular to the vector connecting the centroid of the classes.

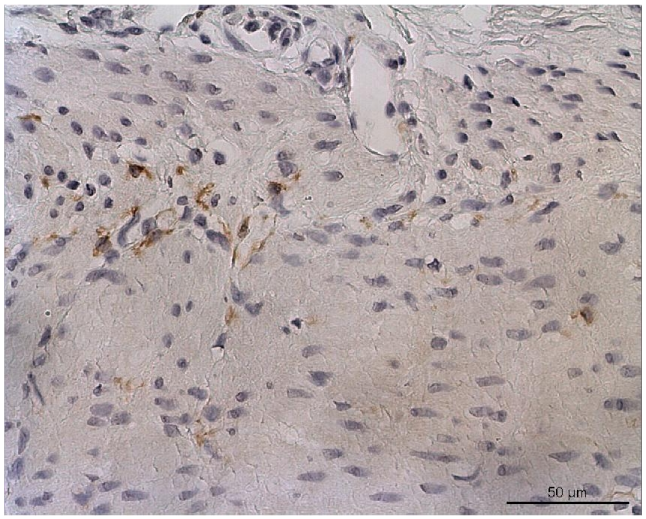

(a) Image captured by the microscope

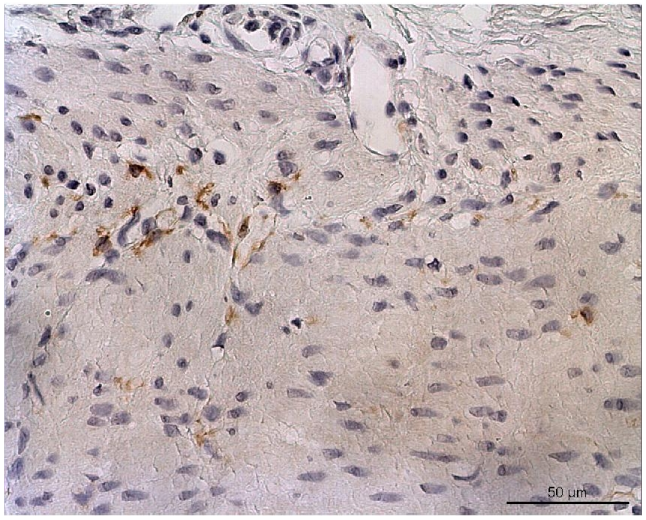

(b) Contrast enhanced image

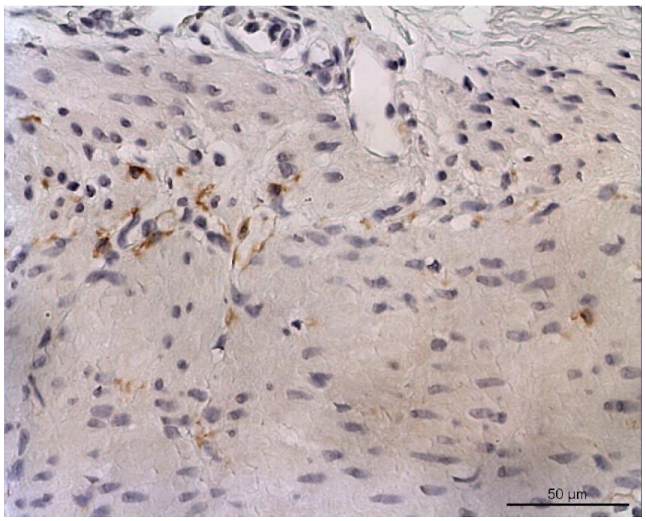

(c) Preprocessed image

Figure 2.4: Preprocessing images

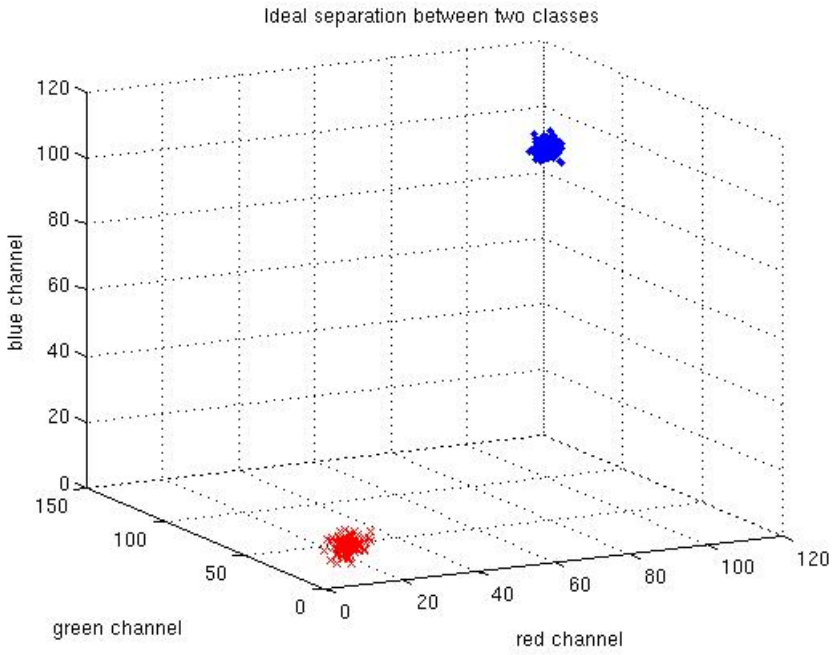

Figure 2.5: Ideal separation between two classes

In this project, the cloud of points representing the Cajal cells is separated by all the other points. The discrimination is done by construction of a vector between the brown color class representing the Cajal cells and the blue cells representing the nucleus. The blue cells are preferred with respect to background pixels because they are represented mostly with blue channel whereas the background is represented with all the three classes of colors (red, green and blue). Thus, discrimination between background and brown cells is more difficult. When the vector separating the two classes of colors is constructed (basis vector), all pixels on the image are projected onto it creating a grayscale image. The basis vector for the projection is chosen in order to maximize the inner product of the Cajal cells and to minimize all the other scalar products of the objects present in the image. The grayscale image is then thresholded, a threshold represents the construction of a hyperplane between two classes of points.

2.3.2 Image projection and threshold

The projection of each pixel of the image into the new basis (the new reference is formulated in 2.2) is computed as in the formulation 2.3. The pixelwise projection is computed into the RGB color space. Image 2.6 shows a projection of a point onto the new reference basis.

Firstly, the reference vector or the new basis vector is defined. This vector is computed as the difference between an average point representing the Cajal cells and an average point representing the blue nucleus. In the interface, user selects nine points of each of the two classes and for each class an average vector representing it is constructed. Then, the reference vector is defined as the difference between these two vectors, formula 2.2 reports this computation.

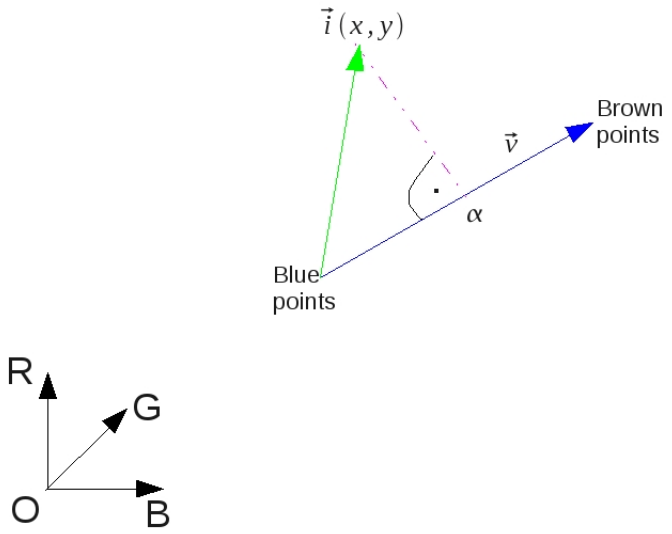

Figure 2.6: Vector projection

$$\overrightarrow{v} = \overrightarrow{c} - \overrightarrow{n} \tag{2.2}$$

where $\overrightarrow{v}$ represents the reference or the new basis, $\overrightarrow{c}$ is the average vector representing the Cajal cells and $\overrightarrow{n}$ is the average vector representing the nuclea. Then, each pixel of the image is projected onto this new basis. A pixel in the image is defined as $\overrightarrow{i} = [r, g, b]^T$ and the pixelwise projection is defined as in formulation 2.3.

$$\alpha = \frac{\left\langle \overrightarrow{i}, \overrightarrow{v} \right\rangle}{\|\overrightarrow{v}\|} \tag{2.3}$$

where $\left\langle \overrightarrow{i}, \overrightarrow{v} \right\rangle$ represents the inner product between a pixel in the image and the basis vector and $\|\overrightarrow{v}\|$ is the norm of the basis vector.

Figure 2.7 shows the grayscale image produced after the projection of the pixels onto the new basis vector.

In the image 2.7, some of the Cajal cells have only the boundary of the cells on white with the inside of the region to low values (dark pixels). This problem arises from the preprocessing step, more precisely when the contrast is enhanced, dark pixels become darker if they are below the low threshold, resulting in holes onto the projected cells. This problem is avoided by the use of the hole filling filter (ref. chapter 2.4.1.4).

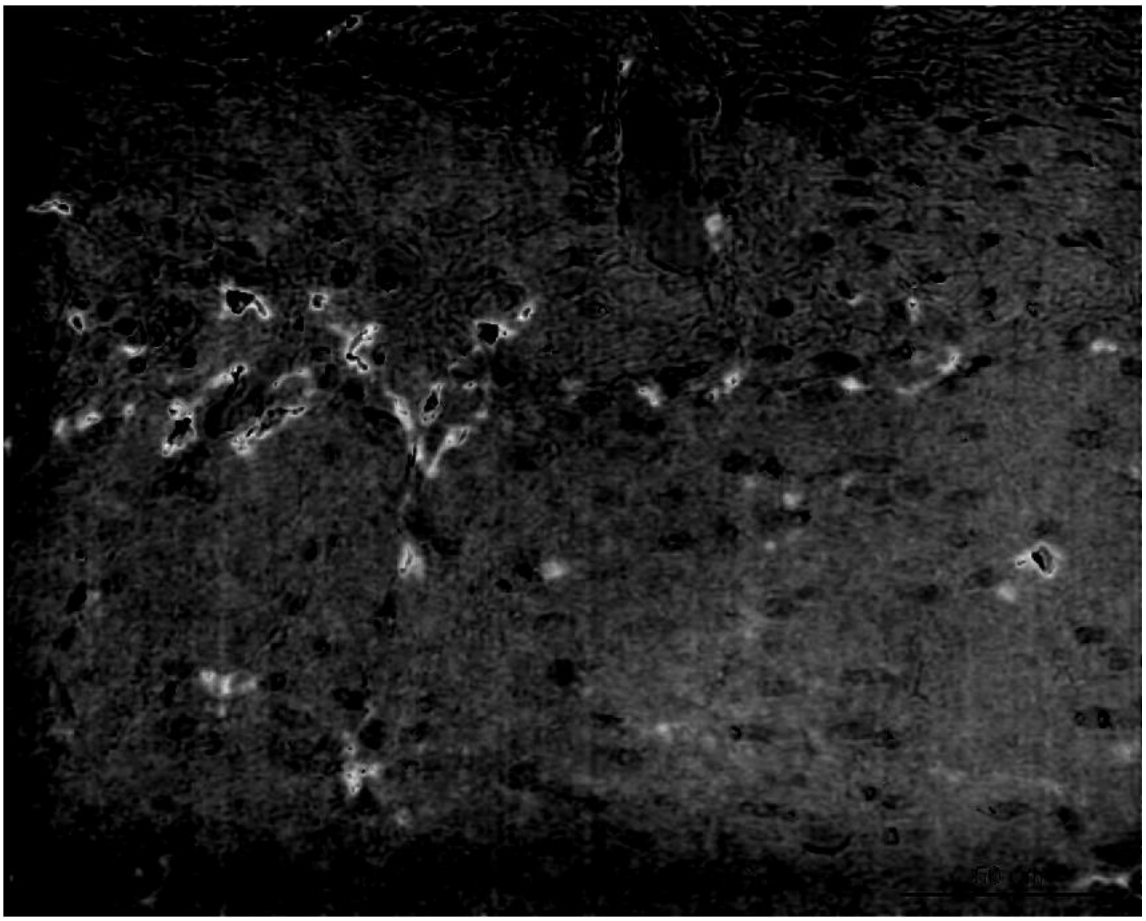

Figure 2.7: Grayscale projected image

After all the pixels are projected onto the new basis, the resulting image as cited above is thresholded to select only the cells belonging to Cajal. Figure 2.8 shows the result after the threshold, this image is no longer grayscale but it becomes binary, where bright spots represent the Cajal cells. This operation is crucial because it can strongly affect the results of segmentation, too low or too high threshold leads to poor segmentation. Remarks : depending on the image, a processing before threshold can be applied in order to remove background areas that have the same color intensity as the Cajal cells. Processing before threshold is discussed in section 2.4.2 because it uses morphological operators. The threshold is computed as in the formulation 2.4.

$$I_{bwCajal} = I_{grayscale} > T \tag{2.4}$$

where $I_{bwCajal}$ is the binary image after thresholding, $I_{grayscale}$ is the projected image, T is the value of the threshold.

After thresholding, morphological operators are applied to increase the quality of the segmentation and to correct small errors belonging to the segmentation process. Subsection 2.4 presents a brief theory of the morphological operators and explains their application in the processing flow

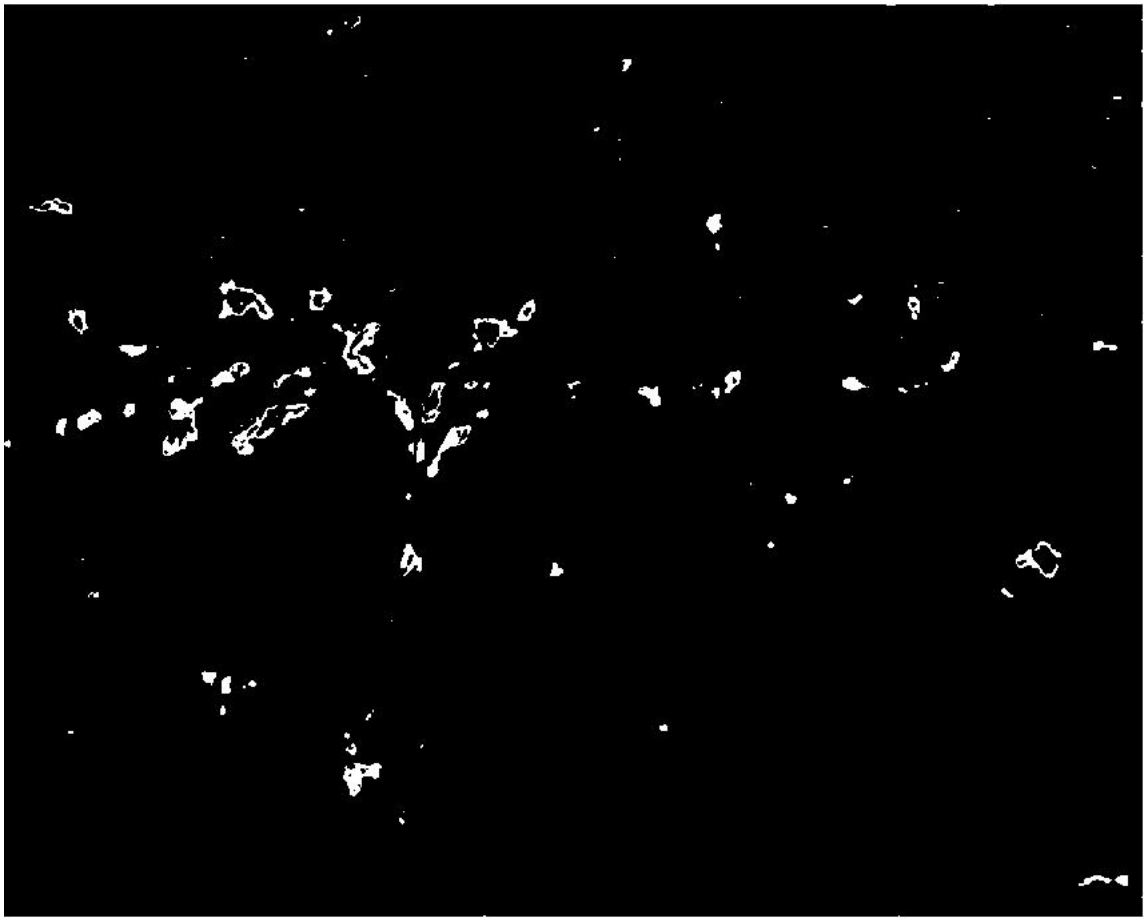

Figure 2.8: Thresholded image

for the Cajal cells segmentation.

2.4 Morphological operators

The mathematical morphology is a tool that deals with form and structure of the image for extracting particular components [2, 17, 18, 19]. Practically, in image processing, morphological filters are used when it is required to preserve shapes that are related to the structuring element. The structuring element is the kernel of the morphological operators. Morphological operators are based on the language of the set theory [19]. The set theory is a branch of mathematics that study sets, which are collections of objects. These operators can be applied on binary or grayscale images. Mathematical morphology is often used in preprocessing or postprocessing, in this case it is used as a postprocessing task.

The simpler morphological operators are the erosion and the dilation, these two operators are complementary and constitute the basis for more complex filters such as opening and closing. The next subsections introduce the theory behind the erosion, dilation, opening and closing operators. Finally, a discussion on the application of the morphological operators for the purpose of Cajal cells segmentation is presented.

2.4.1 Morphological operators theory

This section briefly presents the theory that constitutes the morphological operators. The starting point for the discussion of the morphological filters are the erosion and dilation. These operators are the building blocks for the construction of the opening and closing operators. Then, a discussion on the pixel connectivity is done and the related hole filling operator is presented.

2.4.1.1 Erosion and dilation

The first morphological operator that is presented is the erosion. The effect of this filter onto a binary image is to erode the boundary of foreground objects by a structuring element [17]. The structuring element determines the shape of the foreground objects that the filter can influence and the shape is considered with respect to the origin point of the structuring element. In binary images, foreground regions are considered white pixels. In binary images, erosion is defined in formula 2.5 [10].

$$A \ominus B = \{x \in \mathbb{E} | \, (B)_x \subseteq A\} = \bigcap_{x \in B^s} (A)_x \tag{2.5}$$

where A is the image to filter, B is the structuring element, B^s is the symmetric structuring element and $\mathbb{E}$ is the set of every possible element. The formulation 2.5 indicates that the result of this operation are all the points of the foreground regions that completely contain the structuring element B with respect to its origin. In grayscale morphology, erosion is defined as a minimum filter 2.6 [10].

$$(f \ominus b_0)[k] = \min_{k_0 \in W} \{f[k + k_0] \,|\, (k + k_0) \in \Omega_f\} \tag{2.6}$$

where f is the image, b_0 is the structuring element, k is the index of the image, k_0 index of the structuring element, Ω_f domain of the image and $W = \Omega_b$ domain of the structuring element.

The dilation operator is the complementary of the erosion. The effect of this filter onto a binary image is to dilate the foreground zones (or erode the background) by a structuring element [17]. This operator is defined in 2.7 [10].

$$A \oplus B = \{x \in \mathbb{E} | \, (B^s)_x \cap A \neq \emptyset\} = \bigcup_{x \in A} (B)_x \tag{2.7}$$

where A is the image to filter, B is the structuring element, B^s is the symmetric structuring element and $\mathbb{E}$ is the set of every possible element. The formulation 2.7 indicates that the foreground pixels in the resulting image share common points between the sets A and B. The definition of the grayscale dilation is reported in equation 2.8 [10].

$$(f \oplus b_0)[k] = \max_{k_0 \in W} \{f[k - k_0] \,|\, (k - k_0) \in \Omega_f\} \tag{2.8}$$

where f is the image, b_0 is the structuring element, k is the index of the image, k_0 index of the structuring element, Ω_f domain of the image and $W = \Omega_b$ domain of the structuring element.

2.4.1.2 Opening

Opening is an important morphological operator that is based on erosion and dilation. This operator tends to have similar effects to the erosion but with smaller consequences on the boundary. Generally, this filter is used as an undesired object removal (foreground objects), in example to remove small pixels regions due to the noise. As for erosion and dilation, the functionality of this filter depends on the shape and dimension of the structuring element. This filter applies an erosion followed by a dilation, thus the opening [10] is defined as in formulation 2.9

$$A \circ B = (A \ominus B) \oplus B = \bigcup_{x \in \mathbb{E}} \{(B)_x \,|\, (B)_x \subseteq A\} \tag{2.9}$$

This operator preserves the foreground regions that can completely contain the structuring element while eliminating the other foreground regions. In grayscale it becomes a min-max filter.

2.4.1.3 Closing

Closing, is the complementary filtering of opening. It is an important morphological operator based on erosion and dilation building blocks. This operator tends to have similar results as the dilation, it enlarges the boundary but it is less destructive with respect to the original border of the foreground objects. In general, this filter is used for closing holes of the size of the structuring element on the foreground regions. It is defined as a dilation followed by an erosion [10], thus its mathematical representation is reported in formula 2.10.

$$A \bullet B = (A \oplus B) \ominus B = \left(\bigcup_{x \in \mathbb{E}} \{(B^s)_x \,|\, (B^s)_x \subseteq A^c\} \right)^c \tag{2.10}$$

In grayscale it becomes a max-min filter.

2.4.1.4 Hole filling

This operation is similar to the closing filter because it permits to close holes that are present in the foreground regions of an image. Holes mean background regions completely enclosed into a foreground region [13]. This filter is useful in order to completely connect the inside of each foreground region. Figure 2.13(a) shows the image prior to the filtering and figure 2.13(b) shows the results after the application of this filter.

2.4.1.5 Connectivity and small object removal

The small object removal filter is used as an object removal for foreground regions with areas smaller than a value with a specific connected component. A connected component can be chosen as 4,8 neighborhood and indicates how the pixels are taken into account for the area of the region. An 8-connected component is used for this filter because this criteria is less selective.

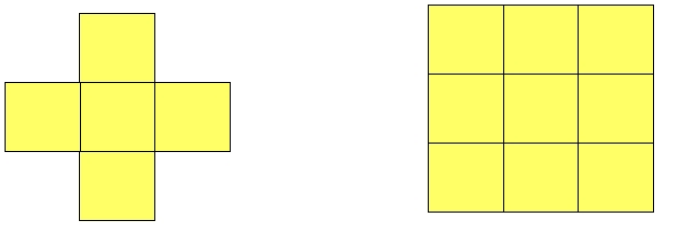

(a) 4-connected component (b) 8-connected component

Figure 2.9: Connected component [10]

2.4.2 Background removal

As cited in the section 2.3.1, certain images require a treatment before thresholding. These images have background area with the same color as the Cajal cells, therefore when segmented these areas are considered as belonging to Cajal cells. Figure 2.15(a) shows such an image. These zones are usually bigger than the Cajal cells, therefore morphological operators can be applied in order to estimate and correct these zones. Figure 2.10 shows the processing steps applied to correct this problem. This treatment is done on the grayscale image.

The operations for the background correction are reported in the equation 2.11 and figure 2.11 shows all the intermediary steps of the schema 2.10. This solution is chosen, because the opening filter within the image estimates the background that should be removed.

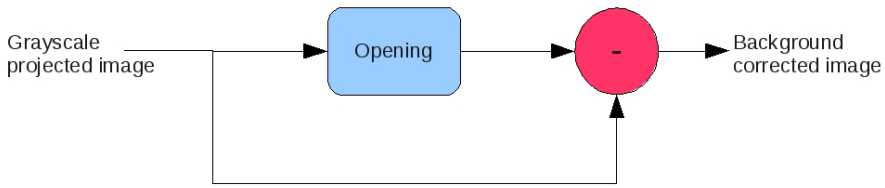

Figure 2.10: Background correction schema

$$I_{backgroundcorrected} = I - [I \ominus SE] \tag{2.11}$$

where $I_{backgroundcorrected}$ is the corrected image, I is the grayscale projected image, $\ominus$ is the morphological opening and SE is the structuring element.

2.4.3 Application to the Cajal cells segmentation

Morphological operators applied to the Cajal segmentation are the last steps before computing the density of these cells. These operators are used as postprocessing filters for increasing the quality of the segmentation. All the steps required for postprocessing are showed in figure 2.12. Figure 2.13 shows the temporary images after each step of the postprocessing operation. The first step consists in filling the holes that can result in the foreground regions (Cajal cells) after the thresholding. This operation is executed via a hole filling filter as cited in subsection 2.4.1.4. Figure 2.13(b) shows the result after this filtering.

Secondly, a closing operator (ref. subsection 2.4.1.3) is applied to gently enlarge and smooth the foreground region of interest. Figure 2.13(c) shows the result after the closing operator. Then a small objects removal filter is applied in order to eliminate small foreground regions that can be considered as noise (figure 2.13(d)). The hole filling operator is used a second time to ensure the complete absence of holes within the foreground regions. Figure 2.13(e) shows the result after this operation.

Finally, the perimeters (figure 2.13(f)) of the binary cells are drawn and superimposed to the microscope image (figure 2.13(g)).

2.5 Validation and results

Validation and the evaluation of the performances of the segmentation is done by comparison of the total segmented areas of the Cajal cells and by visual validation of the results. The reference measurements for the validation process are "manually" segmented by expert operators. In the validation steps, two complete sets and a third partial set of images are used. Only few datasets are used because the "manual" segmentation is time consuming. The selected datasets for the validation are EPFL_PT9B3CKit_2I, EPFL_PT9B3CKit_2J and part of EPFL_PT9B3CKit_2H.

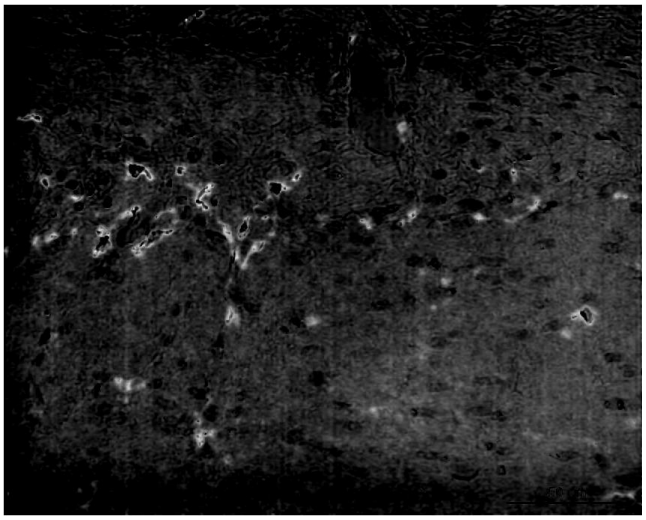

(a) Grayscale projected image

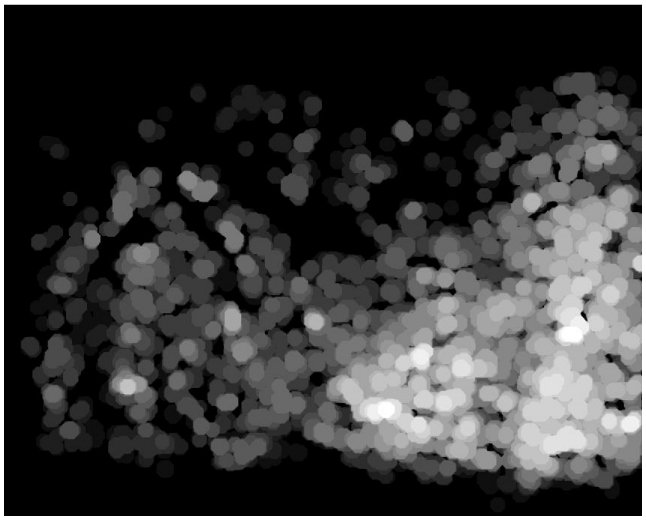

(b) Background estimation

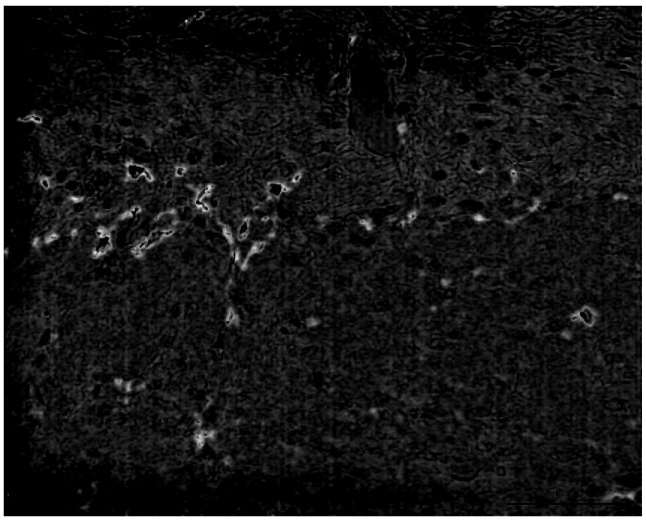

(c) Background corrected image

Figure 2.11: Background correction

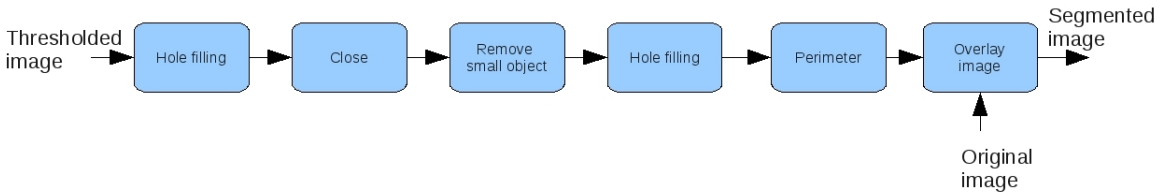

Figure 2.12: Morphological processing flow

These datasets are selected because the Cajal cells are well contrasted and therefore can be easily discriminated with respect to the othe cells.

Two expert users have measured the Cajal cells in three different sets of images as cited above. The measurements of the experts are reported in the table 2.1 under the column Ref. 1 and Ref. 2. The column μ_{ref} reports the avarage areas between the two references. The SA column of this table shows the values of the measurements made by the developed software. The last two columns of the table 2.1 report the deviation with respect to the mean for reference 1 and for "semiautomatic" measurement. Mean computation is reported in formula 2.12 and formulas 2.13 and 2.14 show the deviation for the expert user and for the "semiautomatic" measurement.

$$\mu_{ref} = \frac{ref.1 + ref.2}{2} \tag{2.12}$$

$$\sigma_E = \frac{|\mu_{ref} - ref.1|}{\mu_{ref}} \tag{2.13}$$

$$\sigma_{SA} = \frac{|\mu_{ref} - SA|}{\mu_{ref}} \tag{2.14}$$

$$\tag{2.15}$$

where μ_{ref} is the mean of the references, $ref.1$ and $ref.2$ are the measurements done by expert users, SA is the measurement made by the developed application, σ_E is the deviation of the $ref.1$ from the reference mean in % and σ_{SA} is the deviation of the "semiautomatic" method from the reference mean in %.

The deviations σ_E and σ_{SA} are similar in all the evaluated cases. The maximal deviation of the "manual" segmentation reaches about 16% with respect to the mean. On the other hand, the maximum for the "semiautomatic" segmentation is around 20%. The figure 2.14 shows the image EPFL_PT9B3CKit_2J_40x_A "manually" and "semiautomatically" segmented. Although the "semiautomatic" segmentation performs quite well in the data reported in the table 2.1, on other sets of images such as EPFL_PT9B3CKit_2C the results are bad.

This situation is pictured in figure 2.15(b). This is due to background areas (figure 2.15(a) shows in green these zones of the image) in the images with the same color as the Cajal cells. This

(a) Thresholded image

(b) First hole filling

(c) Closing image

(d) Remove small object

(e) Second hole filling

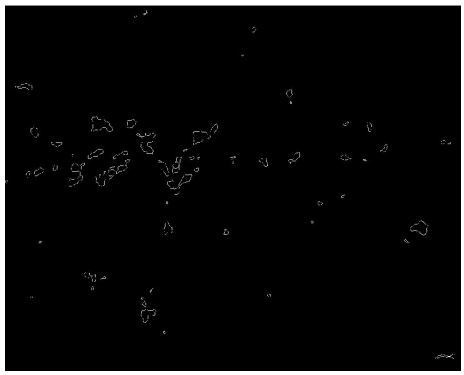

(f) Perimeter

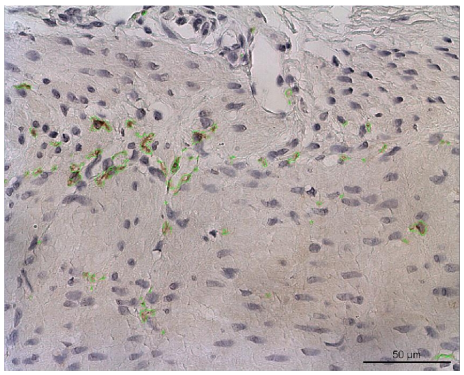

(g) Segmented image

Figure 2.13: Postprocessing results

File name	Areas $[\mu m^2]$				Deviation %	
	Ref. 1	Ref. 2	μ_{ref}	SA	σ_E	σ_{SA}
EPFL_PT9B3CKit_2H_40x_C	501.19	695.26	598.23	**505.79**	16.22	**15.45**
EPFL_PT9B3CKit_2H_40x_D	1037.3	1184.02	1110.66	**1046.2**	6.61	**5.80**
EPFL_PT9B3CKit_2H_40x_E	730.87	779.75	755.31	**697.33**	3.24	**7.68**
EPFL_PT9B3CKit_2H_40x_F	991.28	1001.1	996.19	**943.32**	0.49	**5.31**
EPFL_PT9B3CKit_2I_40x_A	559.85	546.83	553.34	**497.17**	1.18	**10.15**
EPFL_PT9B3CKit_2I_40x_B	430.73	381.35	406.04	**387.34**	6.08	**4.61**
EPFL_PT9B3CKit_2I_40x_C	519.75	436.51	478.13	**445.19**	8.70	**6.89**
EPFL_PT9B3CKit_2I_40x_D	300.17	292.99	296.58	**268.80**	1.21	**9.37**
EPFL_PT9B3CKit_2I_40x_E	528.93	474.61	501.77	**444.52**	5.41	**11.41**
EPFL_PT9B3CKit_2J_40x_A	746.21	690.44	718.32	**572.14**	3.88	**20.35**
EPFL_PT9B3CKit_2J_40x_B	748.14	729.37	738.76	**807.62**	1.27	**9.32**
EPFL_PT9B3CKit_2J_40x_C	675.72	640.39	658.06	**605.12**	2.68	**8.04**
EPFL_PT9B3CKit_2J_40x_D	574.3	683.24	628.77	**649.06**	8.66	**3.23**

Table 2.1: Segmented volumes and error with respect to the reference

problem can be partially mitigated by the application of the background removal as explained in section 2.4.2. Unfortunately, it is not possible to quantify the errors in such cases because there are no "manual" segmentation measurements and therefore the evaluation can only be done by visual inspection.

Another problem that can cause high error on the segmentation is when the Cajal cells cross blue nucleas on the image. This mix of blue cells with brown cells gives to the crossing areas of the Cajal cells strange coloration, such as black and dark brown colors. These mix of colors produce wrong projections on the new basis resulting in wrong segmentation. This effect can be partially mitigated by the application of the morphological operators such as closing filter in the binary image.

Segmentation measurement in both "manual" and "semiautomatic" ways can have a large intravariability due to the fact that Cajal cells do not have well defined boundaries. This can be the case of the image EPFL_PT9B3CKit_2J_40x_C that has been "manually" segmented two times (figure 2.16 shows the two segmented images) by the reference 1, with a deviation from the mean of 9.23 %. The deviation is computed as reported in 2.13. Thus, the evaluation of the boundary cells depends on the experience and on the definition of these cells by the user. The developed program bases the detection of these cells only on the presence of brown pixels whereas the expert user tends to base his segmentation not only on the color of the cells but also on the shape, considering for example filament that goes away from the cells.

2.6 Conclusions

This developed method for the segmentation of the Cajal cells works quite well in datasets where these cells are well contrasted. In datasets where Cajal cells are poorly contrasted, the segmentation

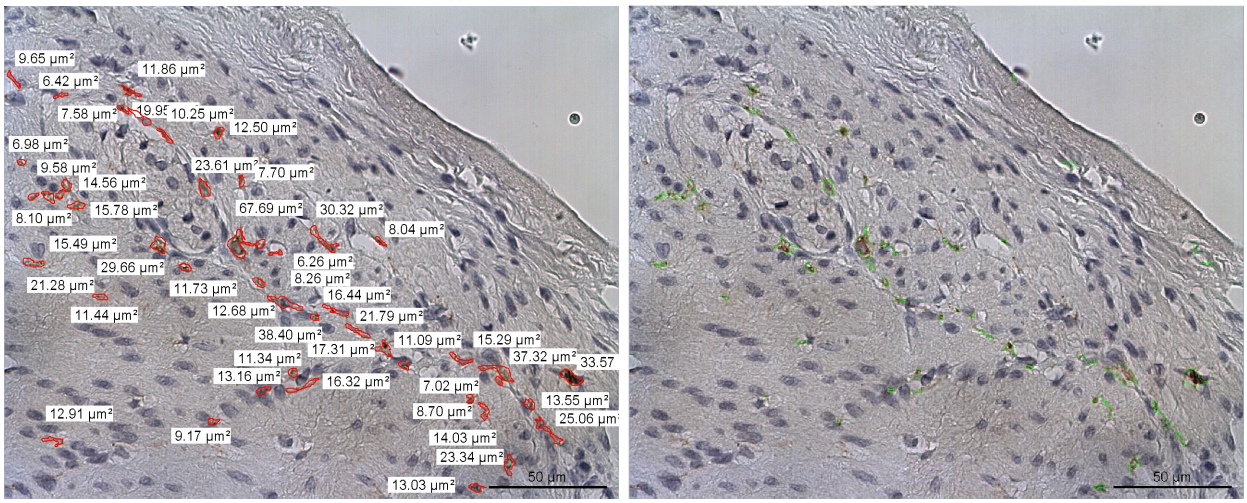

(a) Manual segmented image

(b) Semiautomatic segmented image

Figure 2.14: Manual and semiautomatic segmentation

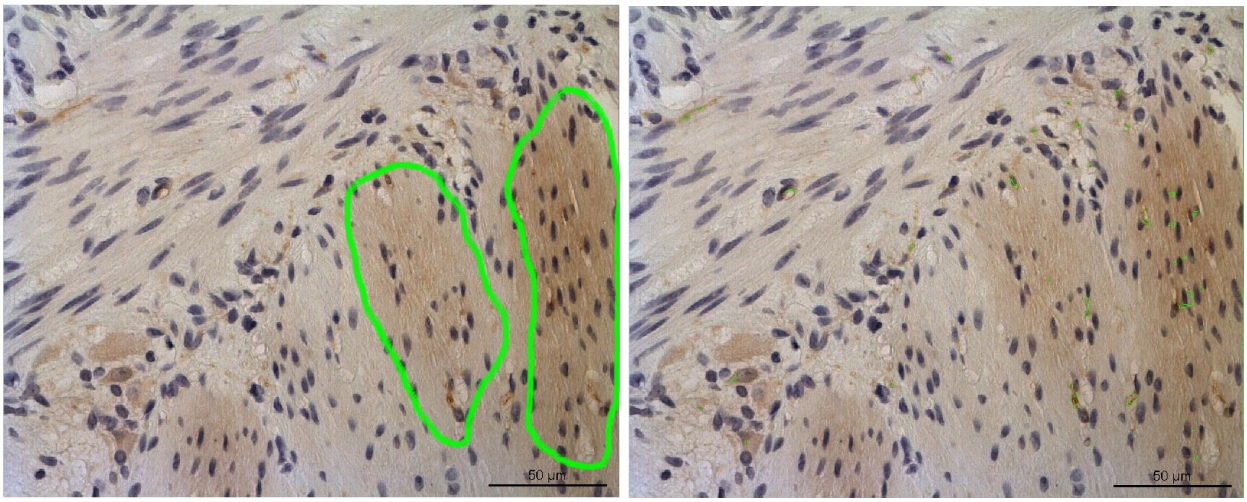

(a) Image EPFL_PT9B3CKit_2C_40x_A

(b) Segmented image EPFL_PT9B3CKit_2C_40x_A

Figure 2.15: Bad segmentation results

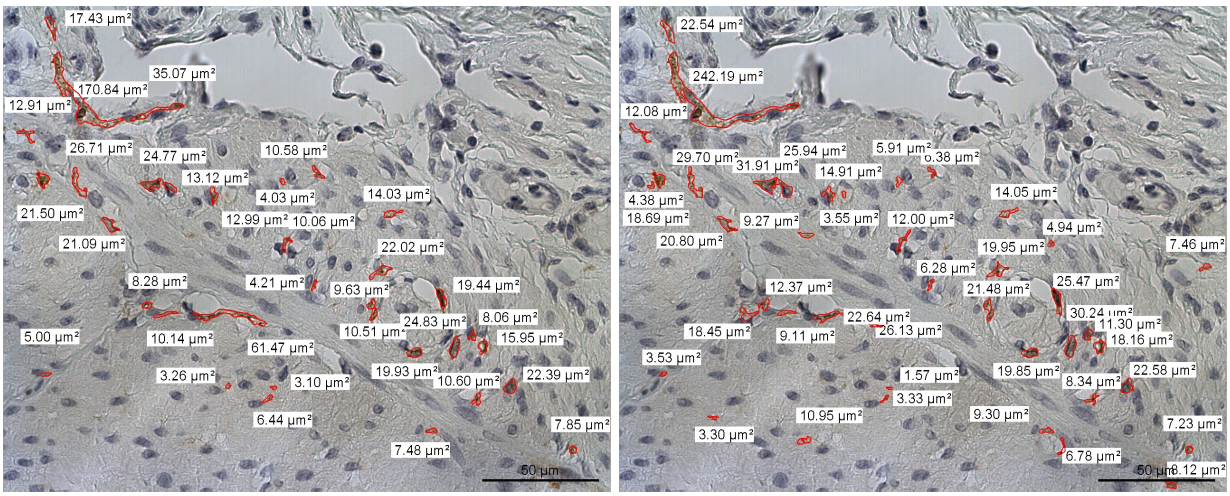

(a) First segmentation of the reference 1

(b) Second segmentation of the reference 1

Figure 2.16: Intravariability of the "manual" segmentation

task performs badly. Unfortunately, these measurements are not acquired due to timing problems, therefore the evaluation of these cases is based only on visual inspection of the segmented images.

The "semiautomatic" way presents a lots of advantages with respect to the "manual" way but also some drawbacks. The major advantage of the developed method is the time consumption, "manual" segmentation requires about 20 to 30 minutes, whereas with the "semiautomatic" methods 5 to 10 minutes are needed. The developed segmentation method is a less decisional task in the sense that it considers only brown color cells instead of users debate about the fact that some cells can belong or not to Cajal. Another drawback of the selected segmentation method is the parameters setting, these steps can strongly influence the results of the segmentation, for example the thresholding phase can have great impact on the results of segmentation, because setting too low or too high thresholds arises in poor segmentation.

A possible solution to the selection of the parameters would be to change the segmentation method in a too high level automatic method, by using techniques such as K-means algorithm [22, 23], principal component analysis [24] or other pattern recognition methods. These methods imply a complete change on the structure of the segmentation, thus a less possible destructive solution can be found in order to limit the changes on the software. These methods can be automatic threshold [7, 25], reduction of postprocessing parameters by increasing the performance of the segmentation task and other similar techniques. These are only ideas of possible changes, more detailed studies have to be made in order to select the correct way to operate within these techniques.

Chapter 3

Image stitching

3.1 Introduction

Image stitching is a well known technique that can be applied in several domains, from amateur photographer to scientific fields. It is used to create a huge image with high details based on sets of small images with high details. This is accomplished by capturing a set of images with high magnification of the region of interested and by stitching all these images together to form a mosaic image. The set of images composing the mosaic require that a certain portion of the neighboring image is shared between them otherwise the process of registration cannot be executed. Figure 3.5(c) shows a mosaic image.

In this project, image registration is used to bind together a set of images that are captured with a high magnification (40x) microscope. In addition, these images are considered to be acquired only by translation, any presence of rotation or other deformation on the dataset provokes a registration failure. This hypothesis is formulated because with the use of the microscope, the specimen can only be translated and therefore all others transformations are inexistent.

Image stitching is computed by translation of a selected image region into the reference image. This technique uses an intensity comparison method called normalized correlation. The correlation technique is chosen among others methods because it is intuitive and performs well in our hypothesis case. The binding process is done by applying masks over the overlapping regions of the images creating a smoothing transition between them. This step is required because the luminosity across the images is not constant.

Image stitching in the case of the Cajal cells segmentation is required for restoring the original area of interest. The stitching of the images is applied after the images are segmented because the segmentation of the mosaic image is more difficult due to the change of luminosity across the image. Section 3.3 presents the application of the image stitching to the Cajal cell segmentation.

3.2 Image stitching

In this project, image stitching deals with three main points :

1. Selection of a rough overlapping region (template image, figure 3.1(c)) on the target image (figure 3.1(b));
2. Compute the correlation between the template and the reference image (figure 3.1(a)) and find the coordinate points in which the images should be stitched;
3. Binding the reference and the target images with masks for smooth transition between them;

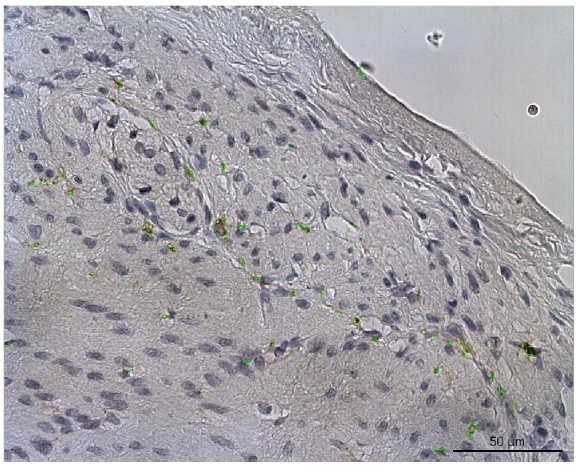

(a) Reference image

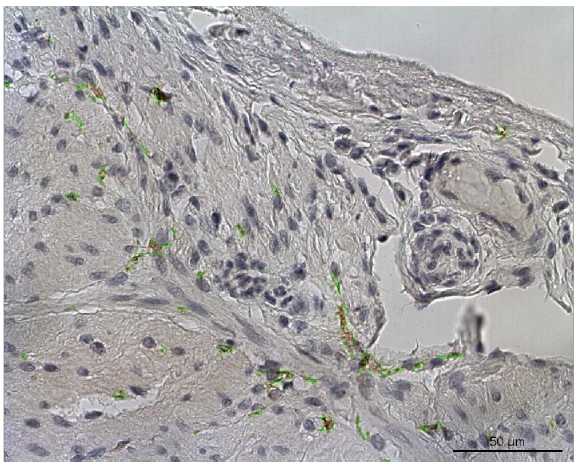

(b) Target image

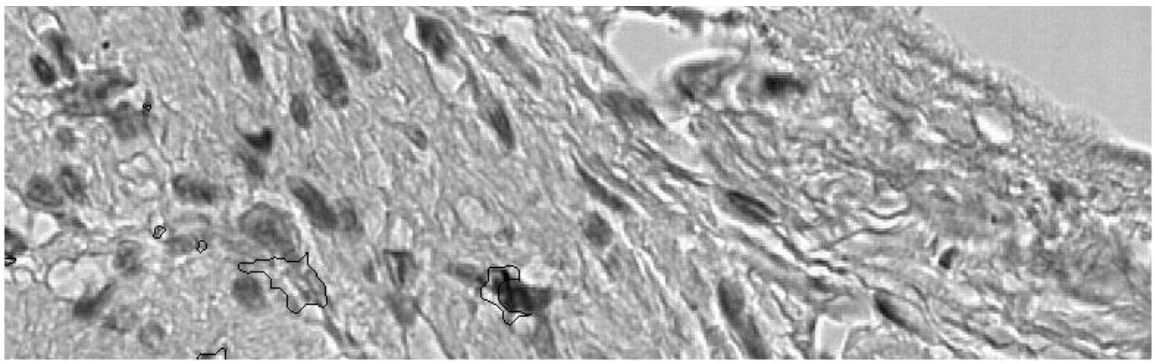

(c) Template image selected from the target image

Figure 3.1: Select rough overlapping region

The following subsections present and motivate all the steps required in order to correctly stitch the images.

3.2.1 Selection of the region of interest

Meanwhile, a completed image can be used, selecting a rough overlapping region allows to slightly increase the performance of the correlation step. Correlation is time consuming, therefore choosing a small region decreases the number of required operations and consequently increases the performance of the system. Other problems can occur using techniques dealing with complete images. Firstly if the overlapping region between the two images is too small, registration can fail because the correlation can not have its maximum at the correct place (i.e if a single cell is selected instead of a region, the cell has probably more similar points in the image than the region, resulting in a wrong maximum position of the correlation and by consequence a registration failure); secondly if the images have a too high resolution the correlation results can be too small due to the normalization, resulting in a registration failure.

3.2.2 Correlation

As cited in the introduction of this chapter, computing the intensity similarity between the images is done by cross-correlation [6]. This technique computes the intensity metric-similarity between a reference image and a template image by shifting the template image into the reference image as shown in figure 3.2. The normalized cross-correlation between two images is defined as in the Mathworks webpage [12] and is reported in the formula 3.1.

$$\gamma(u,v) = \frac{\sum_{x,y}\left[f(x,y) - \bar{f}_{u,v}\right]\left[t(x-u,y-v) - \bar{t}\right]}{\sqrt{\sum_{x,y}\left[f(x,y) - \bar{f}_{u,v}\right]^2 \sum_{x,y}\left[t(x-u,y-v) - \bar{t}\right]^2}} \tag{3.1}$$

where f is the image, $\bar{t}$ is the mean of the template image, $\bar{f}_{u,v}$ is the mean of $f(x,y)$ in the region under the template.

Normalized cross-correlation is computed on a grayscale image. If an image is RGB, one channel of this image has to be chosen. The similarity measurement returns values between -1 and 1, the two extremas indicate that the images are correlated (similar) and values around zero indicate that the two images are uncorrelated (not similar). Image 3.3 shows the result of the cross-correlation. The x-y coordinate corresponding to the maximum of the correlation indicates the best position where the subtarget image should be stitched. The complete target image is stitched in the y-axis at the position reported in 3.4.

$$y_{start} = y_{peak} - ny - y_{min} + 1 \tag{3.2}$$

$$y_{end} = y_{peak} - ny - y_{min} + ly \tag{3.3}$$

$$y_{coord} = [y_{start}; y_{stop}] \tag{3.4}$$

where y_{start} is the starting point and y_{stop} is the last point where the target image is stitched, y_{coord} range of coordinates where the target image is stitched, y_{peak} y coordinate of the maximum of the correlation, ny size in y of the target image, y_{min} coordinate of the upper left corner of the target image and ly size in y of the reference image. All these coordinates are with respect to the left upper corner of the reference image.

The same computations are used for the x-axis.

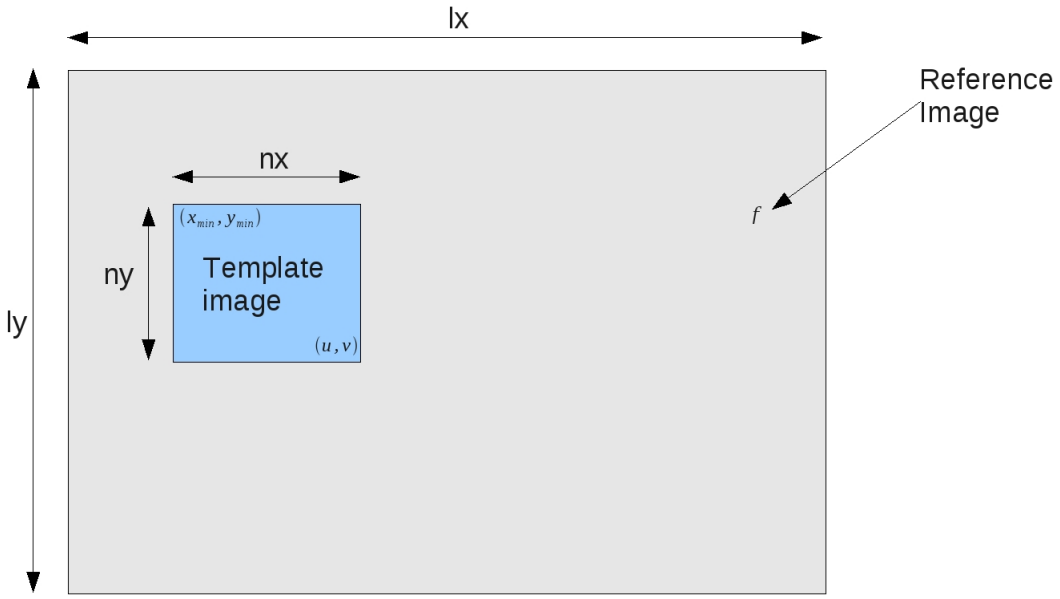

Figure 3.2: Coordinates for cross-correlation

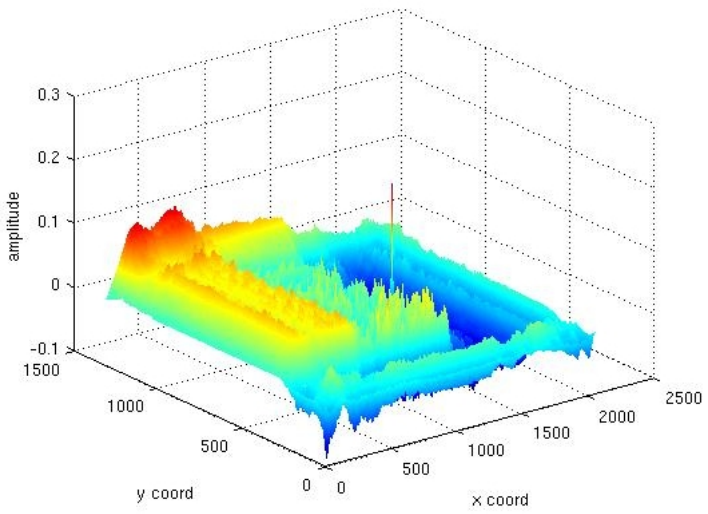

Figure 3.3: Correlation results

3.2.3 Image binding

When the coordinates where to stitch the target image are found, the final step consists in applying a mask to the overlapping region in order to assure a smooth transition between the two images. The source mask (source image with mask figure 3.5(a)) and the target mask (target image with mask figure 3.5(b)) are white gradient masks with opposite direction. The two masks have to sum up to one. Figure 3.4 shows two gradient masks and the sum between them. Figure 3.5(c) shows the stitching with the two masks.

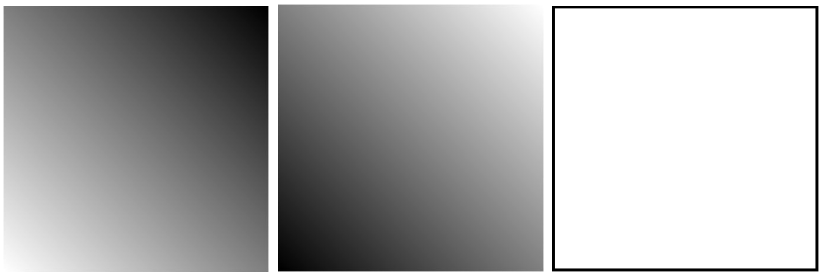

(a) First mask (b) Second mask (c) Sum of the two masks

Figure 3.4: Mask for image binding

Remarks : due to the mask computation the next target image can only be stitched as a neighbour of the current target image. In addition, a constraint on the size of the single images that compose the mosaic image is required. The constraint imposes that the size of all the single images is the same. These remarks belong to the implementation of the stitching function.

3.3 Application to the Cajal cells segmentation

The image stitching in the context of the Cajal segmentation is usefull to restore the complete area of interest for the computation of the Cajal cells. When all the images are stitched together, they form about 1 cm on diagonal of the bowel, with the presence of the two plexus inside the images. Figure 3.6 reports all the steps required in order to correctly stitch the segmented images. This process requires color and a binary image in order to stitch and draw the contours of the Cajal cells on the mosaic image.

All the computation to find the correct positions where to stitch the images are done over the microscope image (color image without segmentation, figures 3.7(a) and 3.7(b)). Once the stitching coordinates are found, the original images as well as the binary (figures 3.7(c) and 3.7(d)) images are stitched. As cited above, the new target image can only be stitched as a neighbour of the current target image, this is due to the mask computation. On the overlapping region of the color images a mask is applied as cited in the subchapter 3.2.3. On the other hand, on the overlapping region of the binary images an "OR" binary operator is applied (figure 3.7(f)). This operator is used to take into account possible bright spots that are present in one image and absent in the

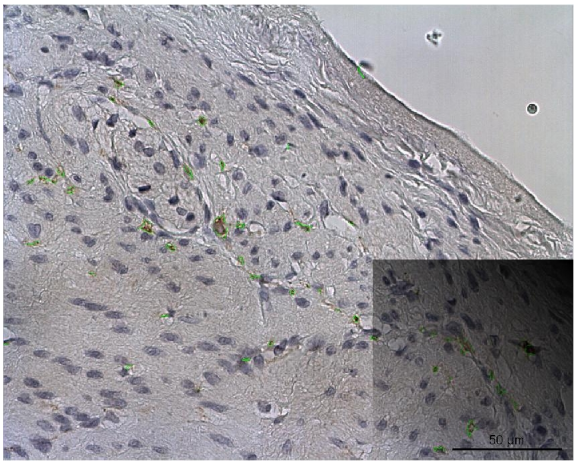

(a) Source image with mask

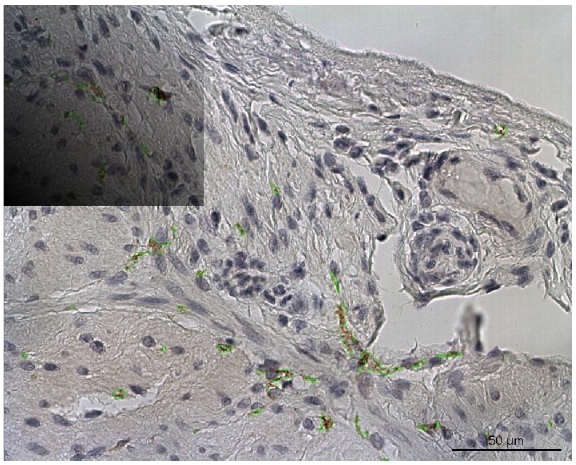

(b) Reference image with mask

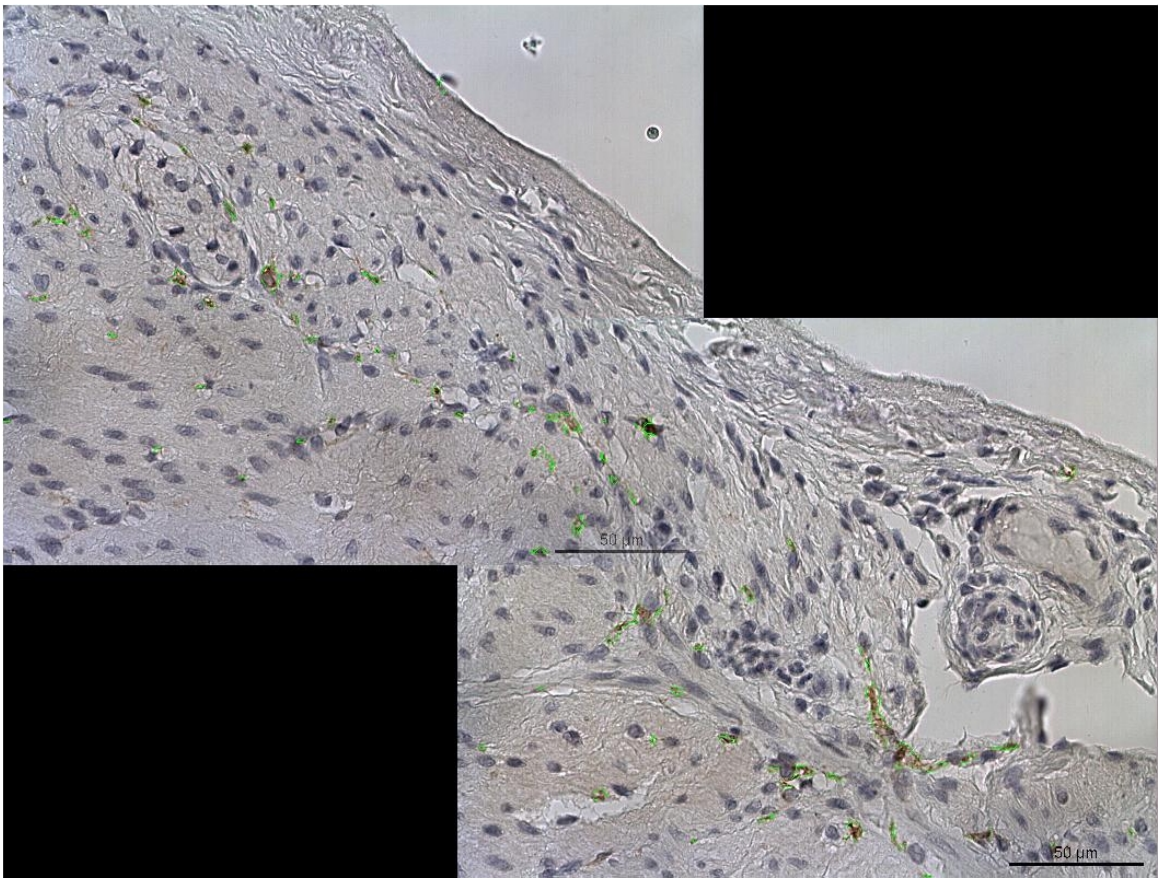

(c) Mosaic image

Figure 3.5: Source and target image with masks

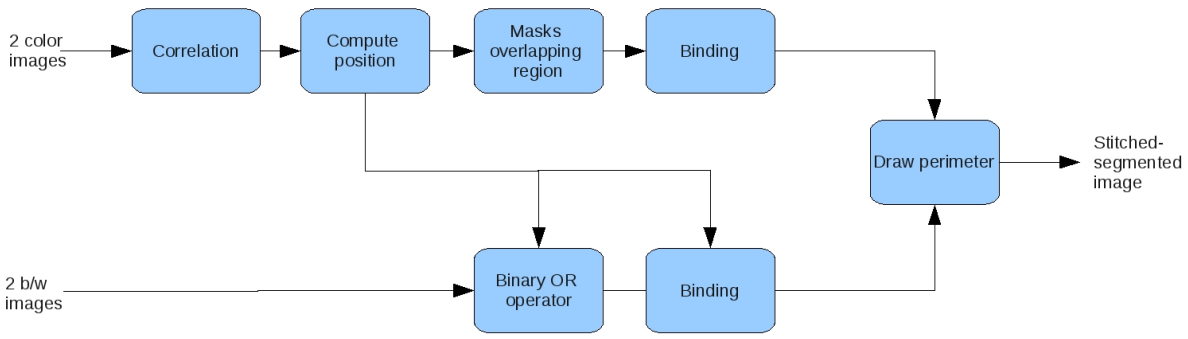

Figure 3.6: Workflow for Cajal stitching

another one. On the binary image, contours of the bright spots representing the Cajal cells are drawn. Next, the color image and the binary image are superimposed to form the new mosaic segmented image.

3.4 Results and conclusion

The suggested approach for image stitching is a good compromise between the efficiency and the easiness from a theoretical and practical point of view. The intensity similarity measurement by the normalized cross-correlation is the easiest method of registration because it computes in a direct way the similarity between the images. There are several drawbacks that limit the use of this technique such as the variation of the luminance between the different images, the noise present in the images and the fact that this method can only be used with translation, any other transformation is not allowed.

The cross-correlation method used in this project is evaluated from a subjective point of view by saying if the images are well stitched (figure 3.8(a)) or not (figure 3.8(b)). Generally, this method works quite well in all datasets of Cajal cells with some exception. The negative cases are due to the lack of information or details in the shared region or too small overlapping region such that the peak of the correlation is not in the correct position.

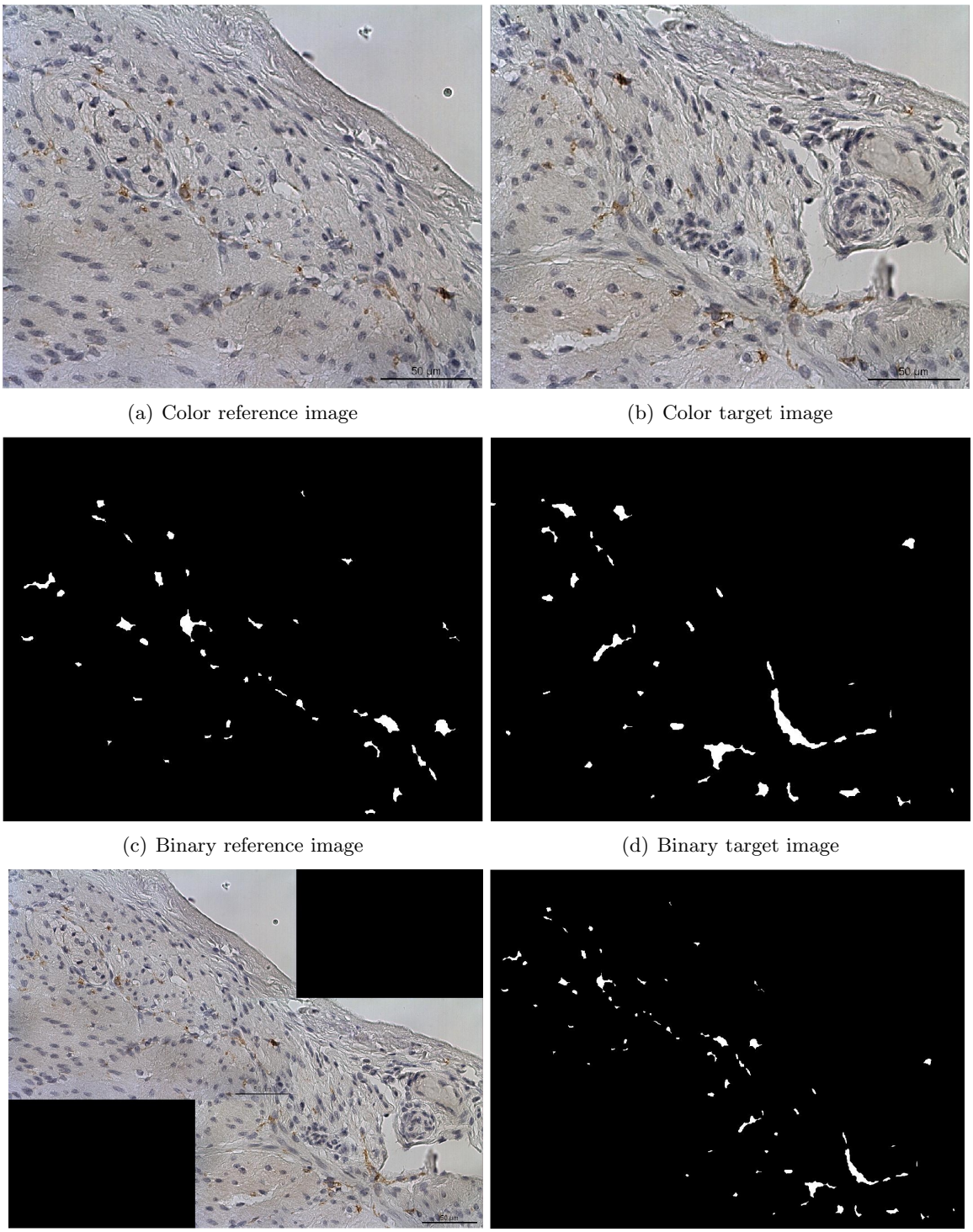

(a) Color reference image

(b) Color target image

(c) Binary reference image

(d) Binary target image

(e) Color mosaic image

(f) Binary mosaic image

Figure 3.7: Temporal images for Cajal stitching

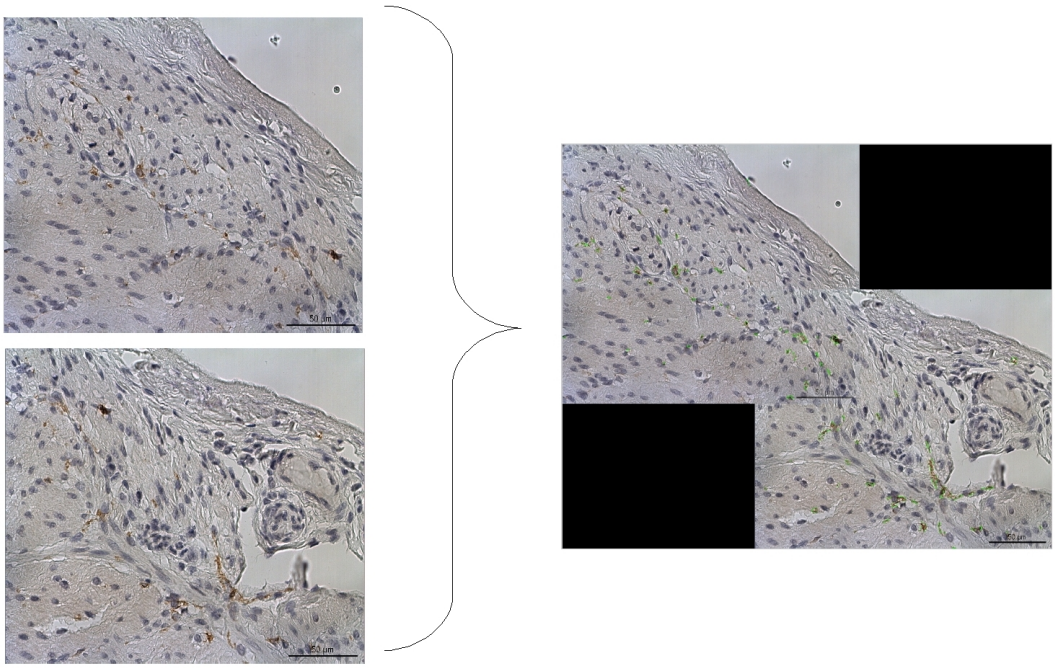

(a) Correctly stitched images

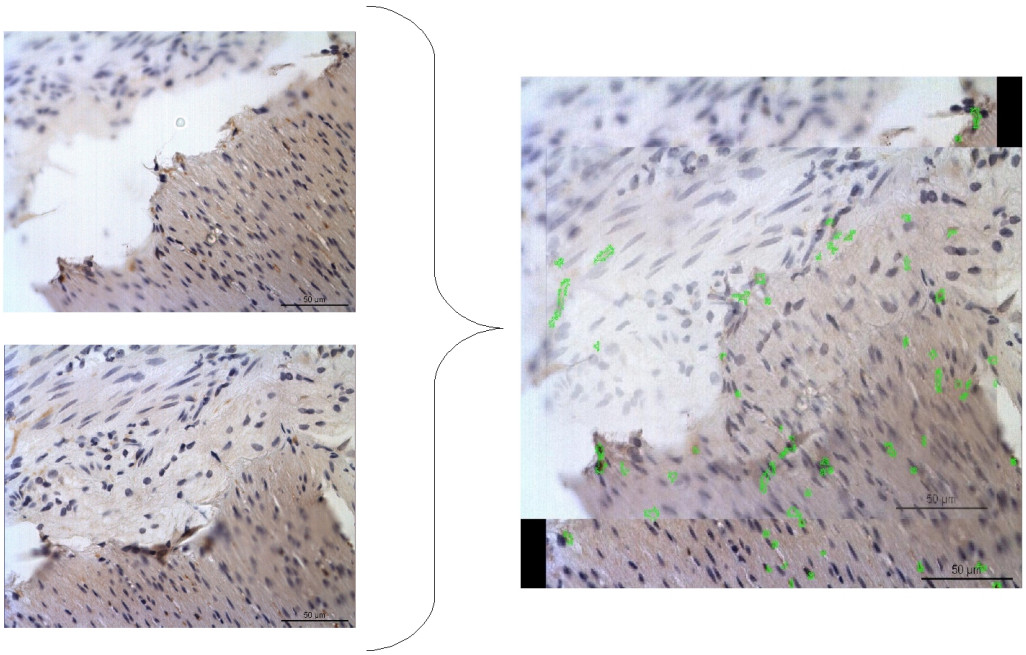

(b) Not correctly stitched images

Figure 3.8: Correctly and not correctly stitched images

Chapter 4

Density computation

The evaluation of the Cajal cells can be done in two different ways : based on the segmented mosaic image or on the single segmented image. The choice of the image in which the densities of the Cajal cells should be computed is dependent on the interest of the user. In addition, two types of measurements of the Cajal cells can be computed, the first measurement is the ratio between the area of the Cajal cells and the total area of the image (section 4.1) whereas the second measurement is the ratio between the area of the Cajal cells and the length of the line (section 4.2) that passes in between the two plexus all along the image.

4.1 Area ratio

The ratio of the areas can be a good measurement of the presence of the Cajal cells but it also presents several drawbacks. Firstly, as cited in 1.2.1, the Cajal cells are in between the myenteric and the submucous plexus, the first plexus has a constant area in all the images whereas the second plexus has an irregular shape resulting in a not constant area across all the images. In addition, this plexus can be stretched in the specimen and by consequence this area is less regular along all the images. Secondly, in the case of the mosaic images, the total area of these images can have huge fluctuation between them (depending on how the images are stitched or how big the overlapping regions are), resulting in a not constant ratio between the different sets of images. Therefore a comparison between them makes no sense. Table 4.1 illustrates the total area of three different datasets.

Dataset	Area $[\mu m^2]$
EPFL_PT9B3CKit_2H_40x_ABCDEF	10693
EPFL_PT9B3CKit_2I_40x_ABCDE	8894.8
EPFL_PT9B3CKit_2J_40x_ABCD	7714.7

Table 4.1: Total area of the stitched images

As a consequence of the fact that this measurement is not adequate, a more constant ratio should be used. This new measurement could be the linear ratio as presented in the next section. Figure

4.1 shows the computed result on a single and a mosaic image. The resulting density can be saved into an Excel file.

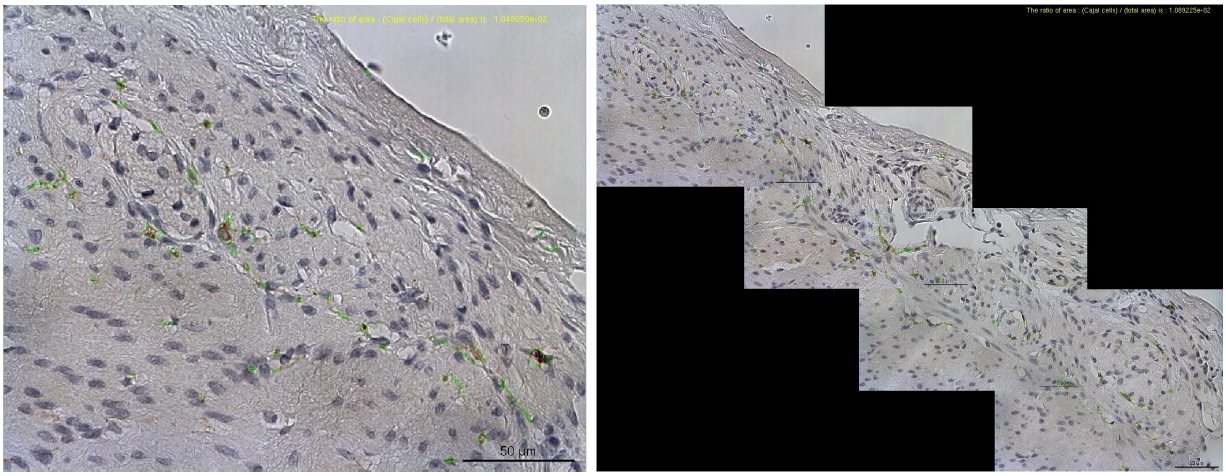

(a) Single image area ratio

(b) Mosaic image area ratio

Figure 4.1: Area ratio

4.2 Linear ratio

The linear ratio is the ratio between the area of the Cajal cells and the length line that passes through the two plexus of the image. This line does not depend on the areas of the two plexus and generally it is supposed to be more constant than the area across all the images. The variability of this measurement depends not only on the length of the region between the two plexus but also on how the control points of the line are selected. Figure 4.2 shows the results on a single and on a mosaic image. The resulting density can be saved into an Excel file.

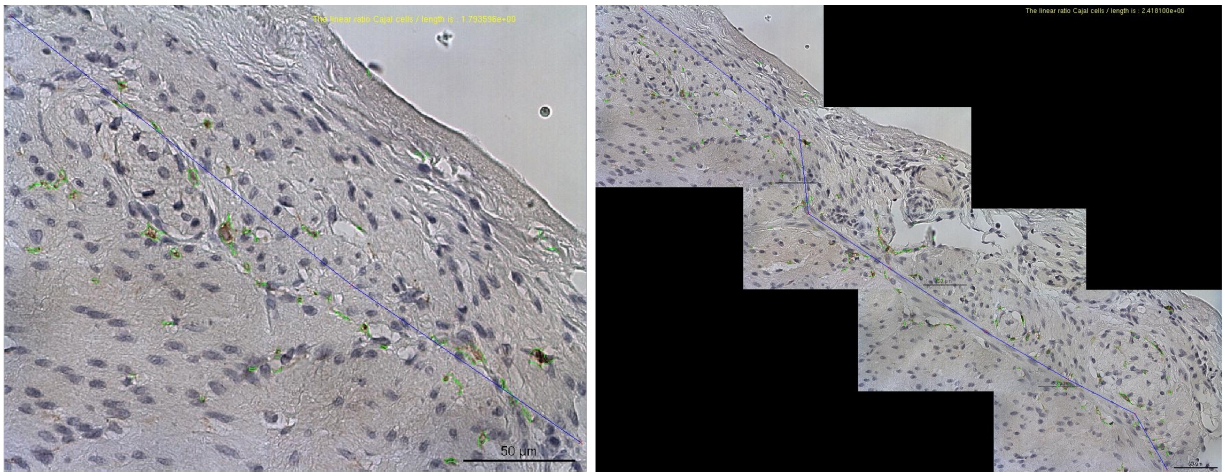

(a) Single image linear ratio

(b) Mosaic image linear ratio

Figure 4.2: Linear ratio

Chapter 5

Segmentation GUI

This section briefly explains the graphical user interface (GUI) developed for the segmentation, image stitching and densities computation. A graphical user interface with tab panels is chosen because it allows to regroup single programs with completely different functions into an unique GUI. The user interface is developed in Matlab with an external library named "uitabpanel" [20] that allows usingF tabs inside the Matlab figures.

5.1 Main and segmentation tabs

The main tab is created for an introduction of the program and indicates the tools present in the different tabs of the interface. Figure 5.1(a) shows the main tab of the GUI.

The segmentation tab allows to load, segment and save the results of the Cajal cells. All the steps that are described in the sections 2.2 to 2.4 are implemented in this tab for image segmentation. The allowed file formats for the input images are ".JPG", ".PNG" and ".TIFF" and the output file format on which the segmentation is saved is a Matlab file ".MAT". This file contains the original image, the segmented image, the binary image and the area of the original image. All these additional variables are required in the next steps, for example for image stitching and densities computation. This is the reason why not only the segmented image is saved. To have more information on how to use this tab, please refer to the segmentation chapter on the HTML help of the graphical user interface. Figure 5.1(b) shows the segmentation tab.

5.2 Stitching tab

The stitching tab in the GUI permits to stitch together a set of images as explained in the chapter 3. This process needs a ".MAT" file, which contains all the elements cited in the segmentation GUI tab 5.1. Once the process of stitching is completed, the stitched image can be saved in a ".MAT" file. This file contains the saved images and variables that are used in the densities tab : the mosaic image without segmentation, the segmented mosaic image, the binary image representing the cells, the total area of the mosaic image and the x-y coordinate where the last image is stitched. To have

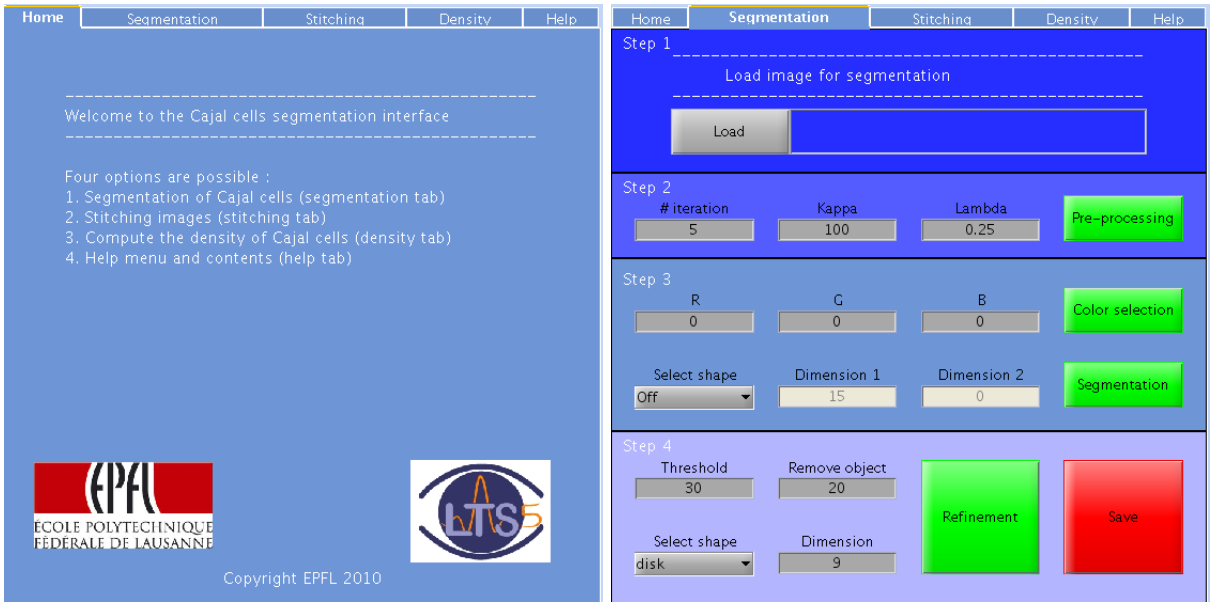

(a) Main tab

(b) Segmentation tab

Figure 5.1: Main and segmentation tabs

more information on how use this tab, please refer to the stitching chapter on the HTML help of the graphical user interface. Figure 5.2(a) shows the stitching tab.

5.3 Density tab

The density tab allows to compute the area density or the linear density of the Cajal cells in a segmented image as cited in the subsection 4. This process requires as input a ".MAT" file containing the information saved in the segmentation or stitching tab. Once all the steps required for the computation of the densities are done, the results of the computation can be saved into an excel file. To have more information on how to compute these densities please refer to the density chapter on the HTML help of the graphical user interface. Figure 5.2(b) shows the density tab.

5.4 Help

This tab allows to consult the HTML help where one can find information on how use the different tabs as well as a description of the parameters that can be modified in order to increase the results of the different operations. Figure 5.2(c) shows this tab.

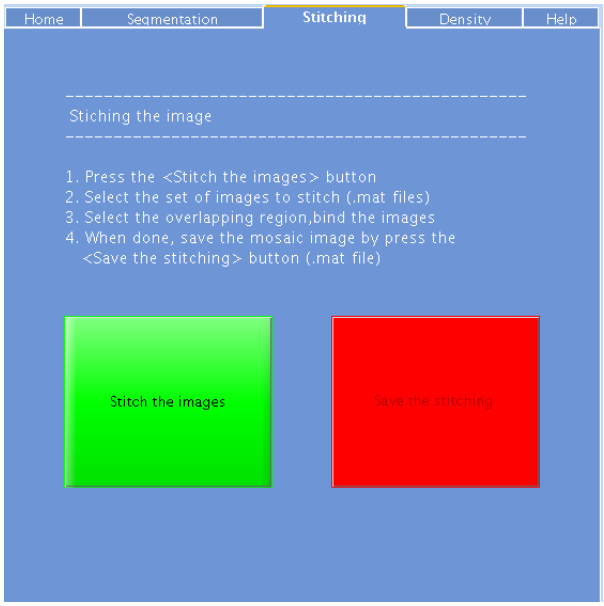

(a) Stitching tab

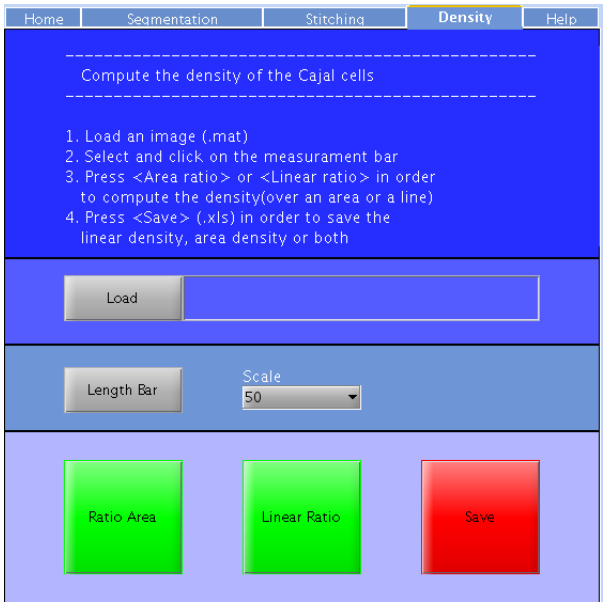

(b) Density tab

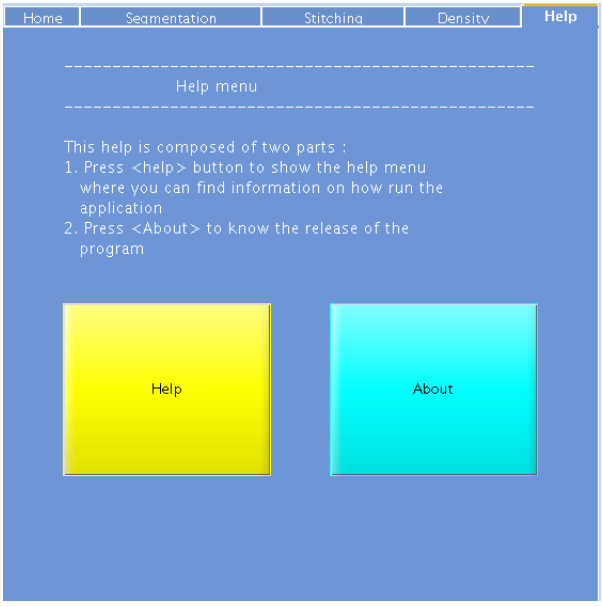

(c) Help tab

Figure 5.2: Stitching, density and help tabs

Chapter 6

Conclusions

The developed segmentation pipeline for revealing the Cajal cells has different performances in function of the images used for the segmentation. Moreover, the quality of the segmentation depends on a lot of factors such as noise, parameter selection and contrast of the images. Therefore a pretreatment has to be done in order to try to uniform the images before segmentation. A postprocessing is also required in order to eliminate possible errors due to the segmentation. The segmentation method as well as all the others treatments require some manipulation by the user, by consequence the segmentation quality can be strongly influenced by the user decision. Globally, if the parameters are well selected the performance of the system are on the same error range of the "manually" segmentation with a maximum deviation of the segmentation with respect the mean of about 20% whereas for "manual" segmentation it is around 15 %. With similar results, a big advantage of the "semiautomatic" method with respect to the "manual" segmentation is the processing time, this is reduced from about 20-30 minutes of the "manual" segmentation to 5-10 with the "semiautomatic" method.

The intensity measurement method for the image stitching performs well in all the datasets except in some where the lack of information on the overlapping region does not permit to correctly compute the normalized cross-correlation. This method becomes more and more consuming on time and on system resources as the images becomes more and more big, therefore a constraint on the possible number of images to stitch exists. The evaluation of the performance of this process is done by visual inspection of the stitched images.

In the density computation, at first thought areas ratio seems more logical and intuitive with respect to the linear ratio but this latter technique is supposed to be more suited for the density computation. The main reason is that the length of the line that passes between the two plexus is more constant across all the images whereas the area of the submucous plexus can be high variable and therefore can highly influence the areas ratio. In the developed program both measurements are possible.

Developing a GUI at first sight can seem an easy task but in reality it is a tough task. Development of a user friendly and easy interface requires a huge knowledge of the ability of the future

users. The developed interface is based on the hypothesis that users do not know anything about image processing, thus the interface should contain as few parameters concerning the process as possible. The developed interface should also contain all the developped application in a single program, this is the main reason why a tab interface has been created.

In conclusion, the main basis for the Cajal segmentation cells are presented in this report but a lot of work remains to be done in order to sensibly increase the performance of the system. In segmentation, to have the first and rough segmented object is easy, but having really good results is not evident and requires a lot of time.

6.1 Future work

The future work should focus on the following points :

- Study more powerful algorithms for image preprocessing in order to increase the result of the segmentation;
- Study more powerful algorithms not only based on the color, but also on possible shapes of the Cajal cells;
- Add the possibility to modify the "semiautomatic" segmentation by "manual" perception of the user on Cajal cells;
- Increase the automation of the segmentation, by modifying the segmentation or the postprocessing tasks;
- Increase the time performance of the system, by increasing the performance of the Matlab routines or for example port all the developed codes into a more performing programming language such C or Java;
- Modify the image stitching routine in order to have a more general way of stitching the images;

List of Figures

List of Tables

Bibliography

[1] Puri, P., *Hirschsprung's disease*, chap.55, pp. 515-533, Second Edition, London : Arnold, 2003.

[2] Gonzalez, R.C., Woods, R.E., *Digital Image Processing*, Third Edition, Pearson Education, 2008.

[3] Gonzalez, R.C, Woods, R.E, Eddinds, S.L., *Digital Image Processing using MATLAB*, Pearson Eduction, 2004.

[4] Solari, V., Piaseczna Piotrowska, A., Puri, P., *Histopathological differences between recto-sigmoid Hirschsprung's disease and total colonic aganglionosis*, Pediatr. Surg. Int. 19 : pp. 349-354, 2003.

[5] Perona, P., Malik, J., *Scale-Space and Edge Detection Using Anisotropic Diffusion*, IEEE Transaction on Pattern Analysis and Machine Intelligence, VOL. 12, NO.7, July 1990.

[6] Rankov, V., Locke, R.J., Edens, R.J., Barber, P.J, Vojnovic, B., *An algorithm for image stitching and blending*, Proceedings of SPIE, Volume 5701, March 2005.

[7] Kittler, J.,Illingworth, J., Fglein, J., *Threshold selection based on a simple image statistic*, Computer vision,graphics and image processing, VOL. 30, pp. 125-147, 1985.

[8] Meyrat, B.J., *Maladie de Hirschsprung (mH) et autres dysganglionnoses*, Slideshow, Service de chirurgie pédiatrique, CHUV.

[9] Meyrat, B.J., *Les dysganglionoses intestinales et maladie de Hirschsprung*, Slideshow, Service de chirurgie pédiatrique, CHUV.

[10] Thiran, J.P., Unser, M.,*Image Processing I and II*, Lecture notes, 8th edition, EPFL, August 2008.

[11] CD117, `http://en.wikipedia.org/wiki/CD117`, March 2010.

[12] Normalized cross-correlation Matlab, `http://www.mathworks.com/access/helpdesk/help/toolbox/images/normxcorr2.html`, March 2010.

[13] Fill image regions and holes, `http://www.mathworks.com/access/helpdesk/help/toolbox/images/imfill.html`, April 2010.

[14] Hirschsprung's disease, `http://http://en.wikipedia.org/wiki/Hirschsprung\%27s_disease`, May 2010.

[15] Hirschsprung Disease Overview, http://www.ncbi.nlm.nih.gov/bookshelf/br.fcgi?book=gene&part=hirschsprung-ov, May 2010.

[16] Imadjust, https://prof.ti.bfh.ch/sha1/Octave/index/f/imadjust.html, May 2010.

[17] Morphology, http://homepages.inf.ed.ac.uk/rbf/HIPR2/morops.htm, May 2010.

[18] Morphological Operators, http://ikpe1101.ikp.kfa-juelich.de/briefbook_data_analysis/node178.html, May 2010.

[19] Mathematical Morphology, http://en.wikipedia.org/wiki/Mathematical_morphology, May 2010.

[20] Uitabpanel, http://www.mathworks.com/matlabcentral/fileexchange/11546-uitabpanel, May 2010.

[21] RGB color space, http://en.wikipedia.org/wiki/RGB_color_space, June 2010.

[22] Clustering K-Means, http://home.dei.polimi.it/matteucc/Clustering/tutorial_html/kmeans.html, June 2010.

[23] K-Means clustering, http://en.wikipedia.org/wiki/K-means_clustering, June 2010.

[24] Principal component analysis, http://en.wikipedia.org/wiki/Principal_component_analysis, June 2010.

[25] Otsu's method, http://en.wikipedia.org/wiki/Otsu's_method, June 2010.